https://doi.org/10.5194/egusphere-2022-899
Preprint. Discussion started: 14 September 2022

Towards long-term records of rain-on-snow events across the Arctic from satellite data

Annett Bartsch[1], Helena Bergstedt[1], Georg Pointner[1], Xaver Muri[1], Kimmo Rautiainen[2], Leena Leppänen[3], Kyle Joly[4], Aleksandr Sokolov[5], Pavel Orekhov[5], Dorothee Ehrich[6], and Eeva Mariatta Soininen[6]

[1]b.geos GmbH, Industriestrasse 1, 2100 Korneuburg, Austria
[2]Finnish Meteorological Institute, Earth Observation Research, P.O.Box 503, FI-00101 Helsinki, Finland
[3]Arctic Centre, University of Lapland, Pohjoisranta 4, 96101 Rovaniemi, Finland
[4]National Park Service, Gates of the Arctic National Park and Preserve, Arctic Inventory and Monitoring Program, Fairbanks, AK 99709
[5]Arctic research station, Institute of plant and animal ecology, Ural branch, Russian Academy of Sciences. Zelenaya Gorka Str., 21, Labytnangi, Yamal-Nenets Autonomous District, Russia
[6]UiT - The Arctic University of Norway, 9037 Tromsø, Norway

Correspondence: Annett Bartsch (annett.bartsch@bgeos.com)

Abstract. Rain-on-Snow (ROS) events occur across many regions of the terrestrial Arctic in mid-winter. Snow pack properties are changing and in extreme cases ice layers form which affect wildlife, vegetation and soils beyond the duration of the event. Specifically, satellite microwave observations have been shown to provide insight into known events. Only Ku-band radar (scatterometer) has been applied so far across the entire Arctic. Data availability at this frequency is limited, however. The utility of other frequencies from passive and active systems needs to be explored to develop a concept for long-term monitoring. Active (radar) records have been shown to capture the associated snow structure change based on time series analyses. This approach is also applicable when data gaps exist and bears capabilities to evaluate the impact severity of events. Active as well as passive microwave sensors can also detect wet snow at the timing of a ROS, if an acquisition is available. Wet snow retrieval methodology is, however, rather mature, compared to identification of snow structure change which needs consideration of ambiguous scattering behaviour. C-band radar is of special interest due to good data availability including a range of nominal spatial resolution (10m-12.5km). A combined approach is therefore considered and tested for C-band (active, snow structure change) and L-band (passive, wet snow). Results were compared to in situ observations (snow pit records, caribou migration data) and Ku-band products. Ice crusts were found in the snow pack after detected events. The more crusts (events) the higher the winter season backscatter increase at C-band. ROS events captured on the Yamal and Seward peninsulas have had severe impacts on reindeer and caribou, respectively, due to crust formation. Temperature dependence of C-band backscatter observable down to -40°C is identified as a major issue for ROS retrieval, but can be addressed by combination with passive microwave wet snow indicators (demonstrated for Metop ASCAT and SMOS). Synthetic Aperture Radar (SAR) from specifically Sentinel-1 (C-band) is promising regarding ice layer identification at better spatial details for all available polarizations. The fusion of multiple types of microwave satellite observations is suggested for the creation of a climate data record, but the consideration of performance differences due to spatial and temporal cover as well as microwave frequency is

https://doi.org/10.5194/egusphere-2022-899
Preprint. Discussion started: 14 September 2022

crucial. Retrieval is most robust north of 65°N, in the tundra biome, where records can be used to identify extremes and to apply the results for impact studies at regional scale.

1 Introduction

Rain-on-snow (ROS) modifies snow properties and can lead to the formation of ice crusts which impact wildlife (incl. muskox, reindeer, fox, crows; Putkonen and Roe, 2003; Forbes et al., 2016; Sokolov et al., 2016; Ehrich et al., 2017) and vegetation (Bjerke et al., 2017) and related fluxes (Treharne et al., 2020). Water percolates through the snow pack impacting energy fluxes, warming the soil beneath (Putkonen and Roe, 2003; Westermann et al., 2011). Events occur across many regions of the Arctic in mid-winter and are sometimes documented through observations of local residents (Forbes et al., 2016). Quantitative accounts are challenging as they require measurements of liquid precipitation and snow properties at the same time (Serreze et al., 2021). Snow pit data which detail layers and hardness can document events, but these are made manually at comparably only very few sites. Air temperature and general precipitation measurements from automatic weather stations usually serve as proxy instead. Such data relate to the trigger of snow structure change but do not reflect the impact. Satellite observations based on microwaves can document the event itself (wet snow) or the change in snow conditions afterwards (Bartsch, 2010b) as grain size increases and often ice crusts form which alter the signal-snow interaction. Such changes occur within a short time compared to general snow metamorphosis (aging of snow) throughout the winter season. Short term snow structure change can be frequently observed with satellites specifically over Scandinavia, northern European Russia and Western Siberia as well as Alaska (Bartsch, 2010b; Serreze et al., 2021). Wet snow (associated with ROS) detection with satellite data requires high sampling intervals, as events can be rather short. The mapping of snow changes afterwards instead of wet snow circumvents this issue but requires the use of wavelengths which are sensitive to changes in snow properties, this means comparably short wavelengths with respect to the typical grain size of snow. Ku-band scatterometer data (2.3cm wavelength) has been shown to reflect snow conditions well in this context (Bartsch et al. (2010a); gridded to 10km nominal resolution) but C-band (5.6cm) acquisitions are much more common and to date operationally available. Forbes et al. (2016) document a ROS events where changes in C-band backscatter (12.5 km nominal resolution) resemble the patterns of a specific event reported through local communities in Western Siberia, southern Yamal peninsula. Events which had severe impacts for reindeer herding have occurred in this region several times in the last two decades. They are suggested to be linked to specific sea ice conditions (longer open water season) (Forbes et al., 2016).

Ku-band radar derived potential ROS events are readily available for 2000 to 2009, reflecting the availability period of data from Seawinds on QuikScat (Bartsch, 2010b). This is to date the only circumpolar satellite based record available (Serreze et al., 2021). The Indian Oceansat-2 and Scatsat-1 provide similar records for 2009 to 2013 and from 2017 onward respectively but have not been used for this purpose to date. Readily gridded backscatter data for Oceansat-2 are available through BYU (Brigham Young University, https://www.scp.byu.edu/data.html) for 2009-2015 (resolution enhanced version 2.2 km). C-band radar data from ASCAT (Advanced Scatterometer) is operationally available on multiple platforms (Metop-A to -C) since 2007 (e.g. Naeimi et al. (2012), 12.5 km gridding) and thus of high interest for recent and future monitoring. A continuation of

https://doi.org/10.5194/egusphere-2022-899
Preprint. Discussion started: 14 September 2022

records with C-band might be a feasible strategy as snow structure change after a ROS leads to a sudden increase in backscatter also in C-band observations although at lower magnitude (Bartsch et al., 2010c; Bartsch, 2010c). A C-band scatterometer regional test indicated applicability of the QuikScat approach (Forbes et al., 2016), but the parameter adjustment to this wavelength has neither been justified so far nor have such data been applied for circumpolar retrieval. The continuation with C-band would be beneficial as it has the advantage that similar information is also available from Synthetic Aperture Radar (SAR) with much higher spatial resolution (starting at 10m as for example accessible through the Copernicus Sentinel-1 mission). Temporal sampling of SAR is much lower, but its complementary value for documenting related snow hardness increase should be explored. Wet snow detection with C-band SAR is comparably mature (e.g. Nagler and Rott, 2000; Nagler et al., 2016) and has been investigated in the context of ROS for sites with good data availability (Vickers et al., 2022). Temperature decrease has been, however, also found to increase C-band backscatter at VV polarization (as is operationally available from ASCAT) during frozen conditions (Bergstedt et al., 2018). But so far only the impact of air or soil temperature has been assessed. Comparisons to snow temperature as well as structure are still lacking. The implications when using the same methodology as for Ku-band (Bartsch et al., 2010a) for ROS detection needs to be quantified and method adaptions explored. This includes the combination with data from other sensors and wet snow detection.

With ROS associated snow surface melting has been shown to be captured by passive microwave missions with focus on the detection of an event itself in several case studies (Serreze et al., 2021). Such records are partially of much coarser spatial resolution than the above mentioned scatterometer records but go comparably far back in time. SSMI records (25km) go back to 1979 but have been used so far for description of single events only (e.g. Grenfell and Putkonen (2008)). AMSR-E2 provides higher spatial resolution (12.5km, available since 2002) and has been therefore applied for regional wet snow detection in ROS context in the past (Semmens et al., 2013; Dolant et al., 2016; Sokolov et al., 2016; Pan et al., 2018; Langlois et al., 2017). The wavelengths used by SSMI and AMSR-E2 are even shorter than Ku-band (0.8 – 1.6 cm versus 2.3 cm). L-band passive microwave observations such as provided by SMOS (2010-present, L-band, 23 cm, 50km) have not been used so far in this context but shown to be applicable for wet snow detection (Mousavi et al., 2021, 2022).

The overall aim of this study is to identify rain on snow events which alter snow conditions. The objectives are to (1) gain insight into recent occurrence of rain on snow events across the Arctic, (2) to explore the potential of radar data for building circumpolar long-term data records, (3) to investigate the impact of events on snow properties and (4) to assess the utility of L-band passive microwave observations for ROS detection. Objective (2) is enabled through the modification of the Ku-band scheme for C-band. In situ data not only encompass standard air temperature and snow depth records from an automatic weather station, as used in previous studies, but are extended to snow pit observations (layer thickness and hardness) as well as automatic liquid precipitation measurements. For the first time also L-band passive microwave observations are considered in this context. The added value of the combination of passive and active microwave records is investigated. One previously documented event on Yamal (2013) is revisited and two recent ROS series are analysed in detail with C-band scatterometer as well as L-band passive microwave observations (Yamal and Alaska in 2020 and 2021 respectively). The series of ROS which occurred over Yamal in late 2020 is documented through a dedicated in situ campaign and in addition analysed with C-band

https://doi.org/10.5194/egusphere-2022-899
Preprint. Discussion started: 14 September 2022

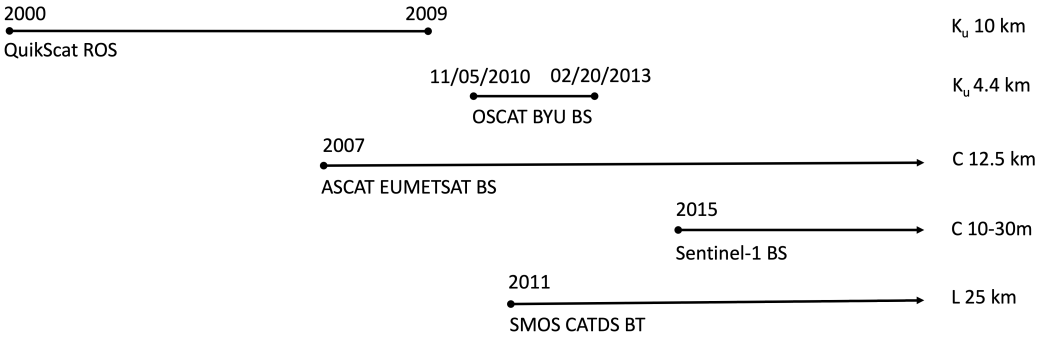

Figure 1. Availability of continuous records from used microwave satellite data, band and nominal resolution. ROS - rain-on-snow product (active microwave), BS - backscatter (active microwave), BT - brightness temperature (passive microwave).

SAR. The potential to provide a measure of severity of a ROS event for wildlife is explored in addition based on caribou migration patterns in Alaska in case of the December 2021 events.

2 Satellite Microwave data

2.1 Ku-band scatterometer

The Quikscat (Ku-band) product of potential ROS events (Bartsch, 2010a) is based on HH polarization acquisitions and starts with winter (November to February) 2000/01 and ends winter 2008/09 (Figure 1) due to instrument failure. The pencil beam antenna design allowed for several measurements per day (Bartsch et al., 2010c) compared to Metop ASCAT (C-band) which provides 80% global coverage only every day in case of one satellite. Oceansat-2 (also referred to as OSCAT) theoretically provides continuity for Quikscat, but the processing used for the ROS product is based on a different scheme (Technical University Vienna) than publicly available for OSCAT (through BYU - Brigham Young University). The type of gridding (full footprint resampling versus partial footprint resampling) differs, leading also to different nominal resolution. A transfer of the QuikScat approach has been nevertheless tested in order to investigate the potential for the production if a longer data record. The so called 'egg' product has been selected (4.4km nominal resolution, Long (2017)). The Oceansat-2 (OSCAT BYU) product starts 5th November 2010 and ends 20th February 2013. The first and last winter (as defined for the QuikScat ROS product) is therefore incomplete. HH polarization is in both cases, QuikScat and Oceansat-2, available from the inner beam acquisitions. Incidence angle differs slightly with 46° and 48.6° respectively.

2.2 C-band scatterometer and Synthetic Aperture Radar

The Advanced Scatterometer (ASCAT) instrument onboard the Metop satellites provides C-band (5.2 GHz) VV-polarized backscatter data sets at a spatial resolution of 25–50 km (Figa-Saldaña et al., 2002). Metop A, B, and C have been launched 2006, 2012 and 2018 respectively. The first records suitable for use start 2007. The data provided by EUMETSAT come in

https://doi.org/10.5194/egusphere-2022-899
Preprint. Discussion started: 14 September 2022

a hexagonal grid (nominal resolution 12.5 km) as part of the soil moisture data product (Naeimi et al., 2009). The provided backscatter value is normalized to a 40° incidence angle. Data are continuously available since 2007, providing global coverage with a temporal resolution of approximately daily observations.

The two earth observation satellites Sentinel-1A (launched in April 2014) and Sentinel-1B (launched in April 2016) have an identical C-band SAR sensor onboard (Schubert et al., 2017). Most land area is monitored with Interferometric Wide Swath (IW) mode (10 m nominal resolution). Near coastal Arctic tundra regions are, however, only covered in Enhanced Wide Swath (EW) mode in medium resolution (40 m) due to requirements for sea ice monitoring. This is specifically the case for the Yamal peninsula, a focus area of this study. Information can be captured in dual polarization (HH+HV or VV+VH; H—horizontal, V—vertical). Mostly HH+HV is available for EW mode in high latitude areas, including Yamal. VV+VH is acquired in IW mode for Scandinavia. GRD (Ground range detected) products were used for this study. GRD products are detected, multi-looked, and projected to ground range using an Earth ellipsoid model (Potin et al., 2014; Potin, 2013).

2.3 L-band radiometer

The SMOS (Soil Moisture and Ocean Salinity) satellite payload instrument MIRAS (Microwave Imaging Radiometer with Aperture Synthesis) observes the Earth at L-band, specifically at bandwidth reserved for radio astronomy (1404 MHz – 1423 MHz). The instrument uses two-dimensional aperture synthesis to provide a series of snapshot images reconstructed from simultaneous measurements of multiple receivers. SMOS observes the target areas at wide incidence angle range (0-60 degrees) and provides fully polarized brightness temperatures at a spatial resolution of 35 to 50 km depending on the measurement geometry. SMOS started the continuous observations in 2010, record use for this study starts however only winter 2011/12 due to data gaps during the first winter. Data used here are from Centre Aval de Traitement des Données SMOS (CATDS), the French ground segment for the SMOS Level 3 and 4 data. CATDS level 3 daily brightness temperatures (L3TB) form the basis for this study. CATDS data are processed from the SMOS L1B products from ESA. The data are binned and averaged into fixed incidence angle classes at five degrees intervals from 0-5 degrees to 60-65 degrees and available on the EASE2 grid projections. The CATDS product includes flags for potential RFI and Sun contamination for users to discard data not suitable for their use.

The vertically and horizontally polarized brightness temperature data are used at the incidence angle range from 45 to 50 degrees. Due to the measurement geometry, there are typically most data available at incidence angles between 25 to 40 degrees. However, at 50 degrees incidence angle the effect of a dry snow cover to the observed signal at vertical polarization is at minimum (see section 4.1, Schwank et al. (2015); Lemmetyinen et al. (2016)). The selected incidence angle range was a trade-off, it provided a good daily coverage and was close to the optimal incidence angle for L-band observations over the snow areas.

https://doi.org/10.5194/egusphere-2022-899
Preprint. Discussion started: 14 September 2022

3 In situ observations and auxiliary data

In situ data comparison and the discussion of specific rain-on-snow events focuses on northern Scandinavia (Finland and Norway), Yamal peninsula (Russia) and Seward Peninsula (Alaska). The Sodankylä site is characterized by boreal forest and all others mostly represent shrub tundra (Figure 2).

3.1 Automatic measurements of meteorologic conditions in northern Finland

Automatic recordings at the Sodankylä experimental site (intensive observation area) include standard AWS data (including air temperature and snow depth) as well as liquid precipitation measurements (referred to as LRI in the following) observed with a Laser Precipitation Monitor (Thies). All these data types are available for the entire length of the analyses period for Metop ASCAT. Daily values are used for this study.

3.2 Snow pit observations - LEENA, DOROTHEE, LABITNANGI team

Three types of snow pit records have been available for the study: weekly, once per season and campaign data. They represent a gradient in northern Scandinavia (#1-3 in Figure 2) and on the Yamal peninsula (#4 in Figure 2).

Of specific interest are snow hardness (Table 1) observations as they reflect presence of ice crusts which can be caused by rain on snow events. The thickness of distinct layers is recorded in addition to a hardness class. The same scheme is used for the sites on Varanger, Saariselkä and Sodankylä.

Regular, mostly weekly observations are made at Sodankylä, as part of an experimental site (intensive observation area - IOA) in 2009-2018 (Leppänen et al., 2016). Since 2018, the snow pit measurement site was relocated to a forested area nearby due to changes in experimental configuration. The IOA site is located within a 40m wide forest clearing, but the associated ASCAT footprint covers peatland to a large extent. A second snow monitoring site is, however, located within a peatland (referred to as BOG in the following). For BOG, snow hardness measurements are not available from all years and at less regular intervals than at IOA, but snow temperature and snow water equivalent (SWE) has been measured in case of most observation dates. The more representative peatland site is therefore used to evaluate C-band backscatter with respect to temperature and SWE. The IOA snow hardness data serve as evaluation of detected events.

Several long-term monitoring sites by Climate-ecological Observatory for Arctic Tundra (COAT, University Tromso) are located on the Varanger peninsula (CITE). Snow pit information is collected every March since 2006. The same snow hardness classification as used at Sodankylä (see Table 1) is used since 2017. The most central site, Upper Komagdalen, has been chosen for comparison as it represents only moderate terrain variability and water fraction within the closest ASCAT footprint. The area represents tundra vegetation and is located at the southern edge of the low Arctic. Multiple sites exist which represent two different types of vegetation: dwarf-shrub heath and meadows adjacent to thickets of erect willow shrubs (up to 2-3m high). Four have continuous records for 2017 to 2020 and represent two data pairs. Each pair has one site near heath and one representing meadow, which are about 80 m apart. The distance between the pairs is approximately 2.2 km. A further site has been established recently near Saariselkä. This site is located between Varanger and Sodankylä and has been previously used

https://doi.org/10.5194/egusphere-2022-899
Preprint. Discussion started: 14 September 2022

Table 1. Overview of terms for snow hardness documentation for available snow pit observations

Site (s)	Term	Hand hardness test	Number	considered as ice crust
Sodankylä, Saariselkä, Varanger	Very soft	Fist	1	No
	Soft	4 fingers	2	No
	Medium	1 finger	3	No
	Hard	Pencil	4	Yes
	Very hard	Knife blade	5	Yes
	Ice	Ice	6	Yes
Yamal	Very fragile	crumbles at the touch of fingers	1	No
	Brittle	easily breaks into small pieces	2	No
	Hard	breaks with fingers with some effort	3	No
	Dense	breaks into large pieces	4	Yes
	Very dense	breaking requires a lot of effort	5	Yes

for L-band passive microwave analyses (Derksen et al., 2017). First snow pits have been made in 2021. It represents tundra but is located close to the treeline. The overlapping ASCAT footprint includes both, tundra and forest.

A snow pit transect of almost 400 km length with samples about every 20 km has been made on the Yamal peninsula, Western Siberia, in February 2021. One of the aims was to document the impact of a series of rain-on-snow events in early winter 2020. Five snow pits have been made per site (one in centre of a square). Snow layers (hardness and thickness) have been measured at all five points. Density was recorded for the central point only. The snow hardness classification slightly differs from the Scandinavian sites. Two of the classes can be associated with ice layers compared to three classes at the other sites. A separate crust documentation is available. Ice and firn crusts are differentiated. Firn crusts consist of frozen individual conglomerates of snow and ice (degree of hardness - pencil or knife test - H4/5; Table 1).

3.3 GPS collar collection for caribou movements in Alaska

From September 2009 to April 2021, female caribou from the Western Arctic Herd, in northwest Alaska (#5 in Figure 2), were instrumented with GPS collars by the Alaska Department of Fish and Game and the National Park Service. All capture procedures were approved by the State of Alaska Institutional Animal Care and Use Committee (permits 2012-031R and 0040-2017-40). From 2009-2019, captures were performed as the caribou crossed the Kobuk River during their fall migration. From 2019-2021, captures were performed using helicopter-based net gunning procedures. Caribou exhibit their lowest movements rates during mid-winter and are relatively sedentary during this season (Joly et al., 2020).

3.4 Further external records

ERA5 reanalyses data (air temperature) have been used for the documentation of events across Yamal as no in situ meteorological records have been available along the snow pit transect. The data was available from the European Centre for

https://doi.org/10.5194/egusphere-2022-899
Preprint. Discussion started: 14 September 2022

Medium-Range Weather Forecasts (ECMWF) and accessed via the Climate Data Store (CDS). Daily maximum, minimum and mean values of 2-metre air temperature were derived from the hourly available 2-metre ERA5 air temperature data.

Landcover information (Landcover CCI) which includes lakes has been used to consistently mask all satellite records. The boundary of the Circum Arctic Vegetation Map (CAVM, Raynolds et al. (2019)) has been used for the separation of tundra for the interpretation of the results. Sea ice concentration records are based on AMSR-E provided through University of Bremen based on Spreen et al. (2008).

4 Methods

4.1 Considerations for C- and L-band use

Microwave interaction at the landsurface is impacted by surface roughness, volume scattering and dielectric properties (e.g. Ulaby et al., 1986; Woodhouse, 2006). Snow and soil properties vary throughout the winter due to structure and phase change what is reflected to a certain magnitude depending on the wavelength used (e.g. Bartsch, 2010c). When a ROS occurs, the snow pack is dry before the event, turns wet during and right after the event until the snow pack refreezes and becomes 'dry' again. Wet versus dry detection is a well explored and common application of microwave observations from satellites (e.g. Nagler and Rott (2000) for C-band and Bartsch et al. (2010c)) for Ku-band. When the liquid water content is increasing in the snowpack, radar backscatter decreases significantly. For L-band passive sensors, such as SMOS payload, the observed brightness temperature at horizontal polarization is significantly decreasing with increasing liquid water content. The vertical polarization signal is not affected as much and may even increase at certain conditions (Pellarin et al., 2016). Wet snow is eventually detected via change detection using thresholds applied to backscatter/brightness of single bands or polarization ratios. The focus of such detection schemes is, however, usually on spring melt. ROS using wet snow from C-band SAR has been investigated for Norway (Vickers et al., 2022) due to very good coverage by Sentinel-1 for this regions. ROS eventually alter the structure of the snow as grain size increases and even ice layers are forming what allows the detection of event occurrence based on subsequent backscatter change at Ku-band (Bartsch et al., 2010a).

The actual magnitude of backscatter change associated with the snow structure change has not been analysed so far as it depends on snow pack history and general landscape properties influencing volume scattering and surface roughness. Ku-band backscatter is also influenced by the amount of snow, the more snow the higher the backscatter (Bartsch et al., 2007). This effect is less present for C-band as the signal penetrates through the snow pack when ice layers are absent (Naeimi et al., 2012). The underlying soil properties may have an effect in this case. When liquid water content is increasing in soils, backscatter increases. Surface roughness also increases the return signal. Roughness may change for example due to tillage, but across the Arctic agriculture is largely absent, so the assumption can be made that roughness stays constant from year to year, but large spatial variations can be observed across different landscapes. This roughness component needs to be considered when absolute temporal variations from different sites are compared with each other. In autumn when the ground freezes, backscatter decreases specifically for C-band due to the drop in dielectric constant (e.g. Naeimi et al. (2012)). For scatterometer data this can be observed to take several weeks as topography within the footprint may vary (Bergstedt et al., 2020). When freeze-up is

https://doi.org/10.5194/egusphere-2022-899
Preprint. Discussion started: 14 September 2022

complete, roughness and volume scattering can be assumed to govern backscatter response. If any other effects are absent, early winter can be used as a representation for surface roughness (Bartsch et al., 2016). There are, however, also other mechanisms than snow structure change which lead to higher values at C-band. Comparisons with soil and air temperature records under frozen conditions suggest a dependence of C-band backscatter (Bergstedt et al., 2020). The lower the temperature the higher the backscatter. This has been found independent from the amount of overlying snow. A sudden drop in temperature (with respect to a chosen time window used in change detection) may therefore show a similar magnitude like the formation of ice layers. So far, this effect has been analysed using absolute backscatter (reflecting roughness, structure/volume and dielectric properties together). To exclude the roughness component, and enable spatial comparability, the location specific surface roughness needs to be determined based on early winter backscatter statistics (minimum) in a pre-processing step. The temperature effect can be then analysed by comparison to in situ snow properties (surface temperature, snow water equivalent).

At L-band the relative permittivity of free liquid water is very high, real part is close to 90 (Maetzler, 2006). This enables many applications, such as detection of liquid water content of soil, and monitoring of soil freeze and thaw cycles. The same applies for detection of ROS events. The emissivity from the frozen soil at L-band is high for both vertical and horizontal polarisation due to the low permittivity (Hallikainen et al., 1986; Maetzler, 2006). The attenuation of dry snow layer on top of the frozen soil is negligible at L-band. A ROS event creates a layer of wet snow on top of the snow cover possibly with some degree of free liquid water within the snow layer. The free liquid water and wet snow decreases the emitted power and thus the measured brightness temperature Tb. The incidence angles around 50 degrees are specifically good for detection of ROS events. Even though a dry snow layer does not attenuate the emission from the frozen soil, it affects the measurements at L-band as a result of impedance matching and changes in the refraction angle at the snow–soil interface (Schwank et al., 2015; Lemmetyinen et al., 2016). At the incidence angles around 50 degrees, the effect is minimal at vertical polarization, while for horizontal polarization the brightness temperature is increased due to the dry snow cover. When soil is frozen and covered with dry snow the normalised polarisation ratio, $NPR = (Tb_{vpol} - Tb_{hpol})/(Tb_{vpol} + Tb_{hpol})$ reaches its minimum value. The wet snow layer and the introduction of free liquid water within the snow layer increases the NPR value. It is therefore possible to set an empirically defined threshold for detection of possible ROS events.

Passive microwave observations as available from SMOS provide two polarizations for a certain frequency and are taken at a range of incidence angles. Band rations are commonly used for wet snow applications. In case of SSMI/SSMR the channel difference between 37V-19V (or 18V) (SSMI/SSMR) is used and in case of L-band (SMOS and SMAP) the normalized polarization ratio (Mousavi et al., 2021, 2022), since wet snow affects the horizontal polarization increasing the V-H difference significantly. The NPR magnitude under dry snow conditions varies spatially. Basic statistics (winter average and standard deviation) which describe dry snow conditions for each grid cell need to be therefore considered for threshold determination (Mousavi et al., 2022).

4.2 Pre-processing of satellite data

ASCAT data available through EUMETSAT as gridded products with 12.5km grid spacing were rearranged into time series for all land area grid points north of 50°N. Data is provided as σ^0 (in dB) values normalized to an incidence angle of 40°. The

https://doi.org/10.5194/egusphere-2022-899
Preprint. Discussion started: 14 September 2022

ASCAT gridding as described in Naeimi et al. (2009) is used. A unique ID is assigned to each grid point (referred to as GPI) of the hexagonal representation. A daily temporal resolution is chosen although data gaps can occur towards south. A (dry/frozen) reference layer has been derived in a first step based on November backscatter (minimum of entire record) for each grid point. The difference to the actual backscatter is then derived and in the following referred to as $\Delta\sigma^0$.

The Oceansat-2 'egg' dataset has been preprocessed similarly to the QuikScat product as described in Bartsch et al. (2010a). This includes the use of HH polarization (inner beam) as well as a static threshold of 1.5 dB for snow structure change identification.

The full polarized SMOS L3 brightness temperature data are available from CATDS in a 25km regular EASE2 polar grid with daily maps (Bitar et al., 2017). This study uses the horizontal and vertical polarized brightness temperatures at incidence angle bin from 45 degrees to 50 degrees. Bad quality data has been masked out based on the standard deviation and accuracy information given in CATDS data for the pixel-wise brightness temperatures and based on the amount of observations that are suspected to be contaminated by the man-made radio frequency interferences (RFI). The Normalized Polarization Ratio (NPR) was determined from the masked data similarly as in SMOS and SMAP freeze and thaw products (Rautiainen et al., 2016; Derksen et al., 2017). In a further masking step, sites with NPR standard deviation larger than 0.02 have been excluded from further analyses. A relatively high standard deviation occurs along coastlines and further regions with high RFI not captured in the CATDS masking and is considered in a later step.

4.3 ROS retrieval

ROS related snow structure changes within the snow pack can be identified by time series analyses of radar backscatter (Bartsch, 2010b). The averaged backscatter of the three days before a specific day are compared with the three days after (dry/frozen conditions in both cases). A certain threshold of backscatter increase needs to be exceeded. So far this threshold has been determined based on single observed events and defined as static (Bartsch et al., 2010a; Forbes et al., 2016), as one value for the entire Arctic. The threshold varies between sensors due to differences in wavelength and noise characteristics. In case of QuikScat (Ku-band) 1.5 dB and for ASCAT (C-band) 0.5 dB have been used. Bartsch et al. (2007) suggest the consideration of location specific noise in case of snow related time series analyses of Ku-band (three times the standard deviation for detection of snow melt). This has been so far not tested for C-band. In general, the noise of the used C-band scatterometer data type (fan beam) is much lower than for Ku-band (pencil beam; Bartsch (2010b); Bartsch et al. (2010c). A threshold of one standard deviation is therefore used. The location specific standard deviation has been obtained from November to February records (Figure 2).

Some regions are characterized by very low standard deviation (e.g. most of eastern Siberia) due to the general aridity and cold temperatures in winter (continuous frozen conditions and low snow depth). The overall difference between the average standard deviation and its standard deviation are considered for this purpose. The resulting value (0.2 dB for $\Delta\sigma^0$) serves as a minimum threshold. The three-day window approach is then applied to the masked dataset to identify sudden change in snow structure.

https://doi.org/10.5194/egusphere-2022-899
Preprint. Discussion started: 14 September 2022

Snow surface temperature measurements from snow pits were used in addition to further analyse the relationship with backscatter as error source. Detected events were eventually compared with weather station records of liquid precipitation (LRI) at Sodankylä in order to investigate false detection due to temperature change.

4.4 Combination with SMOS wet snow retrieval

Eventually, C-Band time series were compared with L-band passive microwave records in order to assess the added value for temperature error correction in the C-band retrievals. NPR increases when air temperature rises above zero degree Celsius, indicating wet snow. NPR level and noise varies from location to location (examples shown for SMOS in Figures 4, 11). This needs to be considered for wet snow detection. Similarly to ASCAT ROS retrieval, a location specific threshold has been defined based on the long-term mean (location specific) and standard deviation (Table 2). Wet snow is assumed only when the NPR exceeds the average plus the standard deviation multiplied by a factor. Mousavi et al. (2022) suggest a factor of 5 for ice sheets. The higher the factor the more events might be omitted. A factor of 3 is applied for seasonal snow based on observations at the Sodankylä reference site (e.g. early November event in 2012, Figure 4). The second step of brightness temperature threshold application as suggested by Mousavi et al. (2022) is omitted as wet snow detection is not the primary indicator but only used in a second step for ASCAT event confirmation.

ASCAT ROS results are eventually tested for wet snow occurrence in SMOS to separate ROS from cold spells. Grid point centres are considered for fusion of the datasets. The closest point is used in each case. A time window of $\pm$ 3 days with data is applied in addition in order to account for timing mismatches as well as SMOS data coverage. The temporal precision is expected to be lower for ASCAT ROS than for SMOS as the algorithm by **?** is based on the assumption that events occur on a single day. When events last longer (e.g. Figure 4), the finally determined date from ASCAT depends also on the magnitude of backscatter change and duration. For the 2013 event on Yamal, two days in a row are detected with wet snow. ASCAT ROS is identified for the day after the second day (Figure 11).

4.5 Pre-processing for evaluation and product cross-comparison

Results are evaluated using snow pit information from specifically the Yamal transect (#4 in Figure 2; one winter) and repeat surveys from Northern Norway and Northern Finland ((#1-3 in Figure 2). In general the presence and thickness of ice layers is used as indicator for a preceding event. Ice layer information (hardness 4, 5 and 6, see Table 1) has been extracted from the records. In case of the Yamal transect, the profile with maximum hardness among the five snow pits per site was selected. This profile was then used for retrieval of crust number and thickness.

We used caribou locations from January 2010-2017 and January 2022 and attributed each location with the value of the cumulative $\Delta\sigma^0$ of events in December 2021. In essence, we compared the intensity of icing experienced by caribou in January 2022 to the intensity of icing they would have experienced at that time if they were located where they were found in years when they migrated to the Seward Peninsula previously (2010-2017). Caribou distributions were generalized by creating Kernel Density Estimates (KDEs) for January 2022, as well as for January 2010-2017 combined, for visualization. The 95% isopleths were derived.

https://doi.org/10.5194/egusphere-2022-899
Preprint. Discussion started: 14 September 2022

To enable satellite product cross-comparison QuikScat, OSCAT and ASCAT/SMOS results were aggregated for specific winters (November to February). For comparison all datasets have been resampled to the 10x10km grid used for QuikScat (see Table **??**. The sum of all events is divided by the number of grid points. Consistent masking for water and glaciated area is used. Greenland is excluded as it is not covered in the QuikScat product. Locations with high RFI in SMOS are also excluded from all products.

4.6 Assessment of polarization differences at C-band using SAR

In order to test further polarizations at C-band, Sentinel-1 HH+HV and VV+VH data have been analysed. Due to the much lower revisit intervals of Sentinel-1 compared to Metop ASCAT, an averaging over a 3-day window is not feasible. The SAR scenes are therefore analysed only in case of detected events with ASCAT and not for event detection itself. These synthetic aperture radar data (SAR) have been preprocessed as outlined in (**?**), the backscatter coefficient σ^0 is derived and normalized to an incidence angle of 40° for comparability with ASCAT. Late October 2020, after freeze-up, is considered for the retrieval of the frozen reference. This reference is compared to acquisitions from December 2020, right after the last potential ROS event before temperatures dropped below -10°C in order to account for temperature effects (Bergstedt et al., 2020). In case of Sodankylä, only one scene before and one after a specific event in 2016 was processed (only pair in Sentinel-1 archive with snow pit data as well as event in between). Results have been re-sampled over a 100m window in order to account for SAR specific noise (speckle). With respect to the high heterogeneity of Arctic landscapes (leading to variations of speckle patterns) and the change of nominal sampling itself, the average was calculated rather than a speckle filter applied.

5 Results

5.1 ASCAT σ^0 and SMOS NPR statistics

C-band backscatter for frozen soil conditions obtained from the beginning of the winter season (frozen reference; minimum derived from all years) varies across the Arctic (Figure 2). The pattern reflects mostly terrain but also vegetation with low values in tundra lowlands (e.g. location #4, around 20dB) and higher values in all mountain areas and forested regions. The standard deviation for mid-winter (November to February) backscatter is less than 0.5 dB for most of the Arctic and on average 0.38 dB. It is higher over forested areas and in regions with a high open water fraction such as parts of the Alaskan North Slope. The sites with snow pit records represent a gradient for the frozen reference and standard deviation. The Sodankylä test site is surrounded by forest and therefore shows medium variation with standard deviation of 0.4 dB as well as a relatively high reference backscatter of σ^0 -13.6dB. The standard deviation is similar for all other in situ and ROS case study regions, but the frozen reference is lower for the Yamal and Varanger peninsulas.

Typical SMOS NPR values are within the range of zero to 0.12, exceeding 0.04 to 0.06 when the snow is wet. The standard deviation is approximately 0.009 at high latitudes (>60N) for the winter months (Table 2).

https://doi.org/10.5194/egusphere-2022-899
Preprint. Discussion started: 14 September 2022

Table 2. Processing steps and results for potential Rain-On-Snow (ROS) identification by fusion of ASCAT backscatter and SMOS Normalized Polarization Ratio (NPR). Events represent November 2021 to February 2022.

Processing step	Input	Time window	Threshold definition	#events >60N	#events >65N
backscatter anomalies based on ASCAT (potential ROS)	backscatter	three days before versus three days after	difference >location specific winter standard deviation, but at least exceeding overall standard deviation (0.2dB)	6495025	3068606
wet snow masking with SMOS	potential ROS dates ASCAT, SMOS NPR	three dates before versus three dates after	NPR > local mean + 3x winter overall standard deviation (0.009)	613561 (9.5%)	332327 (11%)

5.2 ASCAT $\Delta\sigma^0$ sensitivity to snow properties under dry snow and none-ice layer conditions

Only dates with negative temperature and snow hardness H<5 at the BOG site (Sodankylä) were considered. Conditions beyond these thresholds are expected to represent different dominant backscatter mechanisms. ASCAT C-VV backscatter increased up to 4.6 dB above the long-term November minimum between November and February for the dates with snow pit observations (Figure 3). $\Delta\sigma^0$ values ranged mostly between 1dB and 4dB.

In general, 39% of $\Delta\sigma^0$ variation can be explained through temperature (note, a 12.5 km grid is compared to an in situ point measurement, so R^2 might be even higher). A backscatter increase of about 2-3dB can be expected with a snow surface temperature drop down to -25°C. The comparison with snow water equivalent confirms the low influence (compared to temperature) of changes in snow amount on C-VV backscatter.

5.3 Event detection

As an example, a time series of ASCAT, SMOS and the automatic weather station data (air temperature and liquid precipitation) at Sodankylä are shown for winters 2012/13 and 2016/17 in Figure 4. SMOS NPR increases when liquid precipitation is recorded as for mid-November 2016. But not all occasions with liquid precipitation resulted in an increase of NPR or backscatter, as for example in mid-December 2016.

The majority of events detected by ASCAT at this site are related to short term temperature change and have been correctly masked in the second processing step (Table 2) based on SMOS NPR. Such false detection occurred each winter and and outweigh correct identification.

The number of potential events per grid point for the entire Arctic dropped by more than 90% through combination with SMOS data (Table 2). This agrees with observations at Sodankylä. For example, only one out of five of the events could be confirmed with SMOS NPR (Figure 4) at the AWS site in November to February 2012/13. The erroneous detection due to temperature drops can be confirmed with AWS air temperature data in all cases.

https://doi.org/10.5194/egusphere-2022-899
Preprint. Discussion started: 14 September 2022

The general spatial pattern of event occurrence agrees between QuikScat, Oceansat-2 and ASCAT/SMOS results (Figure 5). Northern Europe to Western Siberia experience frequent events as well as near coastal regions along the Bering Sea affecting Alaska as well as Far East Siberia. The magnitude, however, differs between the products. The Ku-band based results (QuikScat as well as Oceansat-2) show more events than the ASCAT/SMOS accounts. Deviations occur specifically over southern forested regions. When compared over tundra, average results are similar between the QuikScat and the ASCAT/SMOS results. This includes the magnitude of events as well as the variability from year to year.

5.4 Characteristics of specific known documented events

5.4.1 Snowpit observations Sodankylä (2012-2019), Varanger (2017-2019) and at Saariselkä (2021)

Snowpit observations have been compared to the final product (masked results) for cases where potential events have been confirmed by wet snow observations. In situ data collected at Sodankylä allow for analyses of specific months for most of the ASCAT period. Detected events at this location occurred specifically in November. The thickness of distinct layers with hardness 4 and/or 5 have been more than 10 cm in years with events (2012 and 2016) (Figure 6). Liquid precipitation has been recorded for the periods of the events in both years (Figure 4). ASCAT C-VV backscatter increased by more than 1 dB for the first events in the season although only little snow was present in both years. Sentinel-1 VV/VH was available before and after the November 2016 event (15.11. and 27.11). Sentinel-1 C-VV backscatter increased more than for ASCAT, by 4.3 dB and in case of VH by 2.1 dB.

The average March cumulative thickness of layers of hardness 4, 5 and 6 varies from year to year at Upper Komagdalen, Varanger (Figure 7). It was lowest for 2018, the only year without events at this site. Only some thin layers with hardness 4 could be observed at Niilanpää in 2021, where also no event was recorded. The snowpits at Varanger and Saariselkä from March represent most of the winter season, but also here, events predominantly occur in November (not shown).

5.4.2 Yamal 2013

A ROS event has been documented for southern Yamal, Western Siberia, in Forbes et al. (2016) with an initial analysis of ASCAT for a small spatial and temporal subset. It was also confirmed based on AMSR-E2 (Sokolov et al., 2016). No in situ measurements are available but reanalyses data and reports from reindeer herders. Reindeer herders reported that the catastrophic ROS event began on 8–9 November 2013 with about 24 h of rain, after which temperatures dropped and remained below freezing for the remainder of the autumn and throughout the winter. Wildlife impacts could be observed in the following for foxes and crows (Sokolov et al., 2016; Ehrich et al., 2017). The event can be also confirmed through SMOS NPR (wet snow; Figure 8). Snow structure change can be detected already on the 7th of November, to the south of Yamal. The ROS extended further to the west on the 10th and 11th of November. SMOS and reanalyses data also confirm the detection issues by ASCAT related to temperature drops after the ROS event. Three out of four detections during winter 2013/14 can be attributed to this phenomenon. The ROS event in November was the only one in midwinter in that season.

https://doi.org/10.5194/egusphere-2022-899
Preprint. Discussion started: 14 September 2022

5.4.3 Yamal 2020

Several documented ROS events occurred between late October and end of December in 2020 across Yamal. Events occurred with partially spatial overlap. The impact on the snow pack has been documented with in situ data along a 350 km transect in February 2021. The snow height was on average 28 cm. Firn (H4 and H5) and/or ice layers (H6) were found at all sites (Figure 9).

Both, satellite and in situ observations, show that the 2020 events have affected most of the Yamal peninsula (Figures 9 and 10). The first warm period at the end of October lasted for several days. It occurred shortly after freeze up, so the starting backscatter level has been comparably low (Figure 11, -15.5 and -17 dB). σ^0 increased by about 1dB after the event in the southern part as well as the northern part of the Yamal transect (Figure 10a and 11). The November 2020 event on Yamal progressed from north to south. It is captured earlier at field point #18 (Figure 11b) than at #3 (Figure 11a). The third ROS phase lasted from end of November to beginning of December and was largely confined to the centre and northern Yamal. σ^0 increased, however, also in the south but no wet snow was detected by SMOS at for example #3. Air temperature also remained at just below zero degree Celsius.

The northern part of Yamal shows the highest number of events and also $\Delta\sigma^0$ in both ASCAT VV and Sentinel-1 HH and HV (Figure 9). This section of the transect has also sites with multiple firn layers or an ice layer (north from point #14). Snow density as well as the crust thickness within the snowpack is also higher in the central and northern part (starting from point #6). Sentinel-1 HH $\Delta\sigma^0$ increases at a similar magnitude like ASCAT VV $\Delta\sigma^0$ from south to north, from about 1 dB to 3-4 dB. Sentinel-1 HV varies more and deviates specifically in the northern part. Cumulative ASCAT $\Delta\sigma^0$ decreases from event to event.

5.4.4 Alaska 2021/2022

The event in central and western Alaska in late 2021 had two phases. An affected area of about 500 x 500 km showed a cumulative backscatter increase of more than 1 dB. The first event started on the 17th of December and the second around the 22nd. They had partial spatial overlap. Sea ice extent declined during the events and the ice boundary retreated beyond the long-term median extent for December (Figure 12).

From 2010-2017, caribou regularly migrated south on their fall migration to the Seward Peninsula, but not since. The distribution of caribou observed during the winter of 2021/2022 was different than 2010-2017. They stayed further northeast (including the Kobuk River plain) and did not disperse to the Seward Peninsula (Figure 12). The Seward Peninsula was among the most affected regions during the two Alaska events in December 2021. If, in January 2022, caribou migrated to where they were found in January 2010-2017, they would have experienced 40.5 % greater $\Delta\sigma^0$ than the caribou actually experienced in January 2022.

SMOS data coverage drops at latitudes below approximately 66°N due to the polar orbit and limited swath size. The Alaska event occurred mostly south of this limit what leads to failures in wet snow detection in addition to the influence of complex terrain and RFI on the SMOS NPR (Figure 12).

https://doi.org/10.5194/egusphere-2022-899
Preprint. Discussion started: 14 September 2022

6 Discussion

The previously suggested static threshold for C-band backscatter increase after ROS (0.5dB, Forbes et al. (2016)) exceeds the average standard deviation of winter time backscatter in the high latitudes (0.38dB, Figure 2). In same regions it exceeds 0.5dB (e.g. Canadian High Arctic). This may lead to false detection with the static threshold. Problematic are also multiple events as in the case of Yamal 2020. The magnitude of backscatter change is decreasing from event to event. The third event lead to an increase of just below 0.5dB (Figures 9 and 11). This third event was most pronounced regarding SMOS NPR (wet snow indicator). First events within the season usually reach about 1.5dB (e.g. Figure 9) although little snow is present (less than 20cm, Figure 4).The observed SMOS NPR winter range agrees with values previously reported for ice sheets (Mousavi et al., 2021).

The comparison to snow surface temperature observations confirms previous analyses which had a focus on soil and air temperature (Bergstedt et al., 2018). The correlation with C-band backscatter can be expected to be more pronounced than for the Sodankylä site for most parts of the Arctic where even lower temperatures occur. The potential increase of backscatter when temperature drops can exceed changes related to snow structure change of single events what underlines the need for a more complex approach than previously suggested for Ku-band backscatter (Bartsch et al., 2010c), a method which relies on short term backscatter increase only.

The differences between the Ku-band results and the combined ASCAT/SMOS events in forested regions (Figure 2) may not be related to noise in the shorter wavelength for most of the Arctic as it is three times lower than the 1.5 dB threshold used for Ku-band (Bartsch et al., 2010b). Instead, polarization may play a role as well as the frequency/wavelength. Currently HH is used for Ku-band and VV for ASCAT. The shorter wavelength of Ku-band leads to a higher sensitivity to changes in the snow pack. More detailed analyses is required to identify the reasons for the differences as well as the correctness of the results of the Ku-band application in forested areas. So far only air temperature measurements have been used for the assessment (Bartsch et al., 2010c; Serreze et al., 2021). Differences among the used Ku-band products can be also expected related to sampling methods. Results may differ for example between the BYU 'slice' and 'eggs' products. BYU also provides an ASCAT product alternative to EUMETSAT (Lindsley and Long, 2016). The 'egg' sampling to 4.45 km and normalization to 0° incidence angle may lead to differences in magnitude and noise and thus also ROS detection. Tao et al. (2022) propose that fusion of QuikScat and ASCAT backscatter records provides applicable time series for vegetation and soil analyses but the suitability might be limited for snow applications.

A general disadvantage of scatterometer and passive microwave observations is the spatial resolution. Near coastal regions are influenced by variations in sea ice and sea surface roughness. Masking is required which leads to exclusion of large parts of the near coast land area. This is more pronounced for SMOS than for ASCAT. Several in situ sites of the Yamal transect could be therefore not used for evaluation (Figure 9). Some mountain regions are also excluded in the SMOS NPR product what may reduce the size of detected ROS as was the case for the Alaska 2021 event (Figure 12). This adds to the issue of data gaps of SMOS due to the polar orbit and swath width at lower latitudes. RFI is permanently high for some regions (see e.g. masked areas inland in Figure 8) and can occur occasionally elsewhere. The impact might be less at lower incidence angles.

https://doi.org/10.5194/egusphere-2022-899
Preprint. Discussion started: 14 September 2022

For larger incidence angles, as used for wet snow observation, the area which affects SMOS observations is larger than for smaller incidence angles. Further investigations are needed to test if the sensitivity of NPR to wet snow is sufficient at small incidence angles in order to fill these gaps.

Additional passive microwave sensor records such as from SSMI/I, AMSR-E and SMAP should be considered to increase the robustness of the wet snow detection. False detection with combination with passive microwave (AMSR-E) at shorter wavelengths has been, however, documented in relation to influence of fog on the snow surface properties (Semmens et al., 2013).

Differences and uncertainties in the location of grid point centres between the wet snow and snow structure change products may lead to lower precision in addition to the grid size issue. Where available, SAR can be used to complement the wet snow retrieval and even provide more detailed information on the actual boundaries of events. C-band SAR could in addition be used to identify snow structure change where temporal sampling is insufficient for reliable wet snow retrieval. Both from Sentinel-1 commonly available polarization options (C-band HH+HV, Figure 9, and VV+VH) show similar $\Delta\sigma^0$ behaviour as ASCAT.

In cases high SMOS NPR without change in ASCAT backscatter can be observed. This occurs for example during November 2012 when further multiple warm phases occurred after the first ROS which lead to a pronounced backscatter increase (Figure 4). ASCAT backscatter varies strongly during soil freeze-up before snow is on the ground. This may lead to false event detection. Also SMOS NPR can increase above the defined threshold during this period. The approach should be therefore only applied for full snow cover. We limited the full Arctic comparison (Figure 5) to November to February to ensure snow presence. This, however, excludes events such as on Banks Island (Putkonen and Roe, 2003) or the first Yamal event in 2020 (Figure 11).

A high LRI without strong change in ASCAT backscatter or SMOS NPR can be also documented for the Sodankylä site. Records are more noisy for both sensors during such periods, but thresholds were not exceeded. For SMOS, this may relate to acquisition timing. Saturation due to the preceding event(resulting in about -10 dB for σ^0) might be a potential reason in case of ASCAT (Figure 4). Events are also not reflected anymore if a certain level (degree of snow metamorphoses) is reached. This is mostly an issue for regions with continuous ice cover which have been excluded from this analyses. Ice sheets show a rather uniform backscatter level at frozen conditions and ROS can be detected through surface melt observations only. Freund and Bartsch (2020) found three major melt events on the Greenland ice sheet in midwinter based on Seawinds Quikscat (26.11.-30.11.2005, 17.11.-21.11.2007 and 01.-04.11.2008). Ice sheets should be included for full Arctic land characterization but only wet snow retrieval applied. Similar issues may apply for sea ice.

Metop ASCAT is available since 2007, but the tested masking scheme is limited to 2011 onward due to later launch of SMOS. A combination with wet snow products from e.g. SSMI/I or AMSR-E could be used to fill the gap. In case of known events, ASCAT results alone could be used as demonstrated for the Alaska event (Figure 12). Care needs to be taken for regional comparisons and climate record data retrieval. An increase of events for the entire Arctic can not be observed with the used records (Figure 5). Regional extremes and recent increase of events can be however identified (Figure 13).

Western Alaska and Western Siberia have been discussed before regarding potential impact on the environment including hydrology and wildlife (Bartsch et al., 2010c; Semmens et al., 2013; Forbes et al., 2016; Sokolov et al., 2016). The two events

https://doi.org/10.5194/egusphere-2022-899
Preprint. Discussion started: 14 September 2022

described for Yamal during the ASCAT period have been the only major events. ROS in this region are rare but have a severe impact especially as they occurred in the first part of the winter what is an issue for reindeer, for example, in the region. All events occurred over the period of several days, progressing spatially. The pattern was different between 2013 and 2020. The direction was West to East in 2013 and partially North to South in 2020. The overall extent and shape (W-E band from Franz-Joseph-Land to the Tassovski peninsula, Figure 8) of the 2013 event agrees with regional AMSR-E2 retrievals by Sokolov et al. (2016). Forbes et al. (2016) suggested a link to sea ice conditions in November for the trigger of such events. Sea ice concentration was lower than average in the proximity of Yamal in both years (Figure 8 and Figure 11), but specifically low towards the west and north in 2020 what might explain to the spatial extent and progression of the ROS. Sea ice extent was also lower than average in case of the Alaska 2021 events (Figure 12), specifically for the second phase. Mean event size for Alaska has been previously quantified as 469 km^2 and at maximum approximately 363,000 km^2 for January based on the QuikScat record 2001–2008 (Wilson et al., 2012). December maximum reached 220,000 km^2 what corresponds approximately to the events observed in December 2021. The situation was unique throughout the ASCAT/SMOS record period (2011-2021) for the Seward Peninsula (Figure 13) and may have contributed to the observed distribution of caribou in the region in early 2022 (Figure 12).

7 Conclusions

Standardized snow pit records, specifically information on ice crusts, have been used for the first time for evaluation of satellite derived rain-on-snow events. The presence of crusts (pencil/knife test) coincides with events detected with the ASCAT/SMOS fusion approach throughout the winter season. In cases without events, no crusts or only thin ones are observed.

The combination of snow structure change and wet snow information provides a compromise regarding constraints due to spatial and temporal sampling as well as frequency. The approach is recommended only for application north of 66°N due to coverage issues of SMOS. There are also discrepancies between C-band and Ku-band in boreal regions for detection of snow structure change which may relate to issues with both data types. Frequency and polarization may play a role, what should be considered in future studies.

The magnitude of specific extreme events can be documented by use of ASCAT alone, without fusion with SMOS. Results can be used for documentation of impacts, as we demonstrated for caribou migration patterns. Low regional sea ice concentration at the timing of events can be observed for all examples, but the number of studied events is too low to infer any linkage. Similarity regarding number of events and spatial patterns between different products (QuikScat, Oceansat-2 and ASCAT/SMOS) can be observed for tundra regions what allows continuous analyses over more than 20 years. Trends for the Arctic cannot be derived but extremes identified and documented.

Data availability. Step 1 (ASCAT only) and step 2 (combination with SMOS) results will be published in seasonally aggregated format and daily maps in due course on PANGAEA.

https://doi.org/10.5194/egusphere-2022-899
Preprint. Discussion started: 14 September 2022

Author contributions. AB has developed the concept for the study, analysed all results and wrote the first draft of the manuscript. HB contributed to satellite data processing and writing of the manuscript. GP and XM contributed to the satellite data processing. KR preprocessed SMOS data and contributed to the manuscript. LL, AS, and PO collected in situ snow data and contributed to manuscript writing. KCJ processed collar records and contributed to the writing of the manuscript.

Competing interests. The authors declare no competing interests

Acknowledgements. The project has received funding under the European Union's Horizon 2020 Research and Innovation Programme under Grant Agreement No. 869471. This work was further supported by the European Space Agency CCI+ Permafrost project.

Oceansat-2 data is obtained from the NASA sponsored Scatterometer Climate Record Pathfinder at Brigham Young University courtesy of David G. Long.

Yamal-campaign data was collected during an expedition organized by the Yamal Government. We thank Aleksandr Volkovitskiy for help in sampling along snow pit transect during the Yamal-campaign.

Rolf A. Ims, Nigel Yoccoz and Hanna Böhner from UiT respectively initiated the collection of snow profiles (RAI and NY) and cleaned the data (NY and HB).

https://doi.org/10.5194/egusphere-2022-899
Preprint. Discussion started: 14 September 2022

References

Bartsch, A.: Spring snowmelt and midwinter thaw and refreeze north of 60N based on Seawinds QuikScat 2000-2009, supplement to: Bartsch, Annett (2010): Ten Years of SeaWinds on QuikSCAT for Snow Applications. Remote Sensing, 2(4), 1142-1156, https://doi.org/10.1594/PANGAEA.834198, 2010a.

Bartsch, A.: Ten Years of SeaWinds on QuikSCAT for Snow Applications, Remote Sensing, 2, 1142–1156, https://doi.org/10.3390/rs2041142, 2010b.

Bartsch, A.: Monitoring of Terrestrial Hydrology at High Latitudes with Scatterometer Data, in: Geoscience and Remote Sensing, New Achievements, edited by Imperatore, P. and Riccio, D., pp. 247–262, Intechweb, Vokuvar, 2010c.

Bartsch, A., Kidd, R. A., Wagner, W., and Bartalis, Z.: Temporal and Spatial Variability of the Beginning and End of Daily Spring Freeze/Thaw Cycles Derived from Scatterometer Data, Remote Sensing of Environment, 106, 360–374, https://doi.org/10.1016/j.rse.2006.09.004, 2007.

Bartsch, A., Kumpula, T., Forbes, B., and Stammler, S.: Detection of Snow Surface Thawing and Refreezing in the Eurasian Arctic Using QuikSCAT: Implications for Reindeer Herding, Ecological Applications, 20, 2346–2358, 2010a.

Bartsch, A., Wagner, W., and Kidd, R.: Remote Sensing of Spring Snowmelt in Siberia, in: Environmental Change in Siberia. Earth Observation, Field Studies and Modelling, edited by Balzter, H., pp. 135–155, Springer, https://doi.org/10.1007/978-90-481-8641-9_9, 2010b.

Bartsch, A., Wagner, W., and Naeimi, V.: The Legacy of 10 Years QuikScat Land Applications - Possibilities and Limitations for a Continuation with Metop ASCAT, in: ESA Living Planet Symposium, Bergen, 2010c.

Bartsch, A., Höfler, A., Kroisleitner, C., and Trofaier, A. M.: Land Cover Mapping in Northern High Latitude Permafrost Regions with Satellite Data: Achievements and Remaining Challenges, Remote Sensing, 8, 979, https://doi.org/10.3390/rs8120979, 2016.

Bergstedt, H., Zwieback, S., Bartsch, A., and Leibman, M.: Dependence of C-Band Backscatter on Ground Temperature, Air Temperature and Snow Depth in Arctic Permafrost Regions, Remote Sensing, 10, https://doi.org/10.3390/rs10010142, 2018.

Bergstedt, H., Bartsch, A., Neureiter, A., Hofler, A., Widhalm, B., Pepin, N., and Hjort, J.: Deriving a Frozen Area Fraction From Metop ASCAT Backscatter Based on Sentinel-1, IEEE Transactions on Geoscience and Remote Sensing, 58, 6008–6019, https://doi.org/10.1109/tgrs.2020.2967364, 2020.

Bitar, A. A., Mialon, A., Kerr, Y. H., Cabot, F., Richaume, P., Jacquette, E., Quesney, A., Mahmoodi, A., Tarot, S., Parrens, M., Al-Yaari, A., Pellarin, T., Rodriguez-Fernandez, N., and Wigneron, J.-P.: The global SMOS Level 3 daily soil moisture and brightness temperature maps, Earth System Science Data, 9, 293–315, https://doi.org/10.5194/essd-9-293-2017, 2017.

Bjerke, J. W., Treharne, R., Vikhamar-Schuler, D., Karlsen, S. R., Ravolainen, V., Bokhorst, S., Phoenix, G. K., Bochenek, Z., and Tømmervik, H.: Understanding the drivers of extensive plant damage in boreal and Arctic ecosystems: Insights from field surveys in the aftermath of damage, Science of The Total Environment, 599-600, 1965–1976, https://doi.org/10.1016/j.scitotenv.2017.05.050, 2017.

Derksen, C., Xu, X., Dunbar, R. S., Colliander, A., Kim, Y., Kimball, J. S., Black, T. A., Euskirchen, E., Langlois, A., Loranty, M. M., Marsh, P., Rautiainen, K., Roy, A., Royer, A., and Stephens, J.: Retrieving landscape freeze/thaw state from Soil Moisture Active Passive (SMAP) radar and radiometer measurements, Renote Sensing of Environment, 194, 48–62, https://doi.org/10.1016/j.rse.2017.03.007, 2017.

Dolant, C., Langlois, A., Montpetit, B., Brucker, L., Roy, A., and Royer, A.: Development of a rain-on-snow detection algorithm using passive microwave radiometry, Hydrological Processes, 30, 3184–3196, https://doi.org/10.1002/hyp.10828, 2016.

https://doi.org/10.5194/egusphere-2022-899
Preprint. Discussion started: 14 September 2022

Ehrich, D., Cerezo, M., Rodnikova, A. Y., Sokolova, N. A., Fuglei, E., Shtro, V. G., and Sokolov, A. A.: Vole abundance and reindeer carcasses determine breeding activity of Arctic foxes in low Arctic Yamal, Russia, BMC Ecology, 17, https://doi.org/10.1186/s12898-017-0142-z, 2017.

Figa-Saldaña, J., Wilson, J., Attema, E., Gelsthorpe, R., Drinkwater, M., and Stoffelen, A.: The advanced scatterometer (ASCAT) on the meteorological operational (MetOp) platform: A follow on for European wind scatterometers, Canadian Journal of Remote Sensing, 28, 404–412, https://doi.org/10.5589/m02-035, 2002.

Forbes, B. C., Kumpula, T., Meschtyb, N., Laptander, R., Macias-Fauria, M., Zetterberg, P., Verdonen, M., Skarin, A., Kim, K.-Y., Boisvert, L. N., Stroeve, J. C., and Bartsch, A.: Sea ice, rain-on-snow and tundra reindeer nomadism in Arctic Russia, Biology Letters, https://doi.org/10.1098/rsbl.2016.0466, 2016.

Freund, K. and Bartsch, A.: Midwinter thaw events over Greenland derived from Seawinds QuikScat 2000-2008, https://doi.org/10.1594/PANGAEA.911298, 2020.

Grenfell, T. C. and Putkonen, J.: A Method for the Detection of the Severe Rain-on-Snow Event on Banks Island, October 2003, Using Passive Microwave Remote Sensing, Water Resources Research, 44, W03 425., 2008.

Hallikainen, M., Ulaby, F., and Abdelrazik, M.: Dielectric properties of snow in the 3 to 37 GHz range, IEEE Transactions on Antennas and Propagation, 34, 1329–1340, https://doi.org/10.1109/tap.1986.1143757, 1986.

Joly, K., Couriot, O., Cameron, M. D., and Gurarie, E.: Behavioral, Physiological, Demographic and Ecological Impacts of Hematophagous and Endoparasitic Insects on an Arctic Ungulate, Toxins, 12, 334, https://doi.org/10.3390/toxins12050334, 2020.

Langlois, A., Johnson, C.-A., Montpetit, B., Royer, A., Blukacz-Richards, E., Neave, E., Dolant, C., Roy, A., Arhonditsis, G., Kim, D.-K., Kaluskar, S., and Brucker, L.: Detection of rain-on-snow (ROS) events and ice layer formation using passive microwave radiometry: A context for Peary caribou habitat in the Canadian Arctic, Remote Sensing of Environment, 189, 84–95, https://doi.org/10.1016/j.rse.2016.11.006, 2017.

Lemmetyinen, J., Schwank, M., Rautiainen, K., Kontu, A., Parkkinen, T., Mätzler, C., Wiesmann, A., Wegmüller, U., Derksen, C., Toose, P., Roy, A., and Pulliainen, J.: Snow density and ground permittivity retrieved from L-band radiometry: Application to experimental data, Remote Sensing of Environment, 180, 377–391, https://doi.org/10.1016/j.rse.2016.02.002, 2016.

Leppänen, L., Kontu, A., Hannula, H.-R., Sjöblom, H., and Pulliainen, J.: Sodankylä manual snow survey program, Geoscientific Instrumentation, Methods and Data Systems, 5, 163–179, https://doi.org/10.5194/gi-5-163-2016, 2016.

Lindsley, R. D. and Long, D. G.: Enhanced-Resolution Reconstruction of ASCAT Backscatter Measurements, IEEE Transactions on Geoscience and Remote Sensing, 54, 2589–2601, https://doi.org/10.1109/tgrs.2015.2503762, 2016.

Long, D. G.: Comparison of SeaWinds Backscatter Imaging Algorithms, IEEE Journal of Selected Topics in Applied Earth Observations and Remote Sensing, 10, 2214–2231, https://doi.org/10.1109/jstars.2016.2626966, 2017.

Maetzler, C.: Dieletric properties of natural media, inThermal Micro-wave Radiation: Applications for Remote Sensing, in: Thermal Microwave Radiation: Applications for Remote Sensing, edited by Clarricoats, P. J. B. and Jull, E. V., vol. 52 of *IET Electromagn.Wave Ser.*, pp. 427–495, Inst. of Eng. and Technol., Stevenage,U. K., 2006.

Mousavi, M., Colliander, A., Miller, J. Z., Entekhabi, D., Johnson, J. T., Shuman, C. A., Kimball, J. S., and Courville, Z. R.: Evaluation of Surface Melt on the Greenland Ice Sheet Using SMAP L-Band Microwave Radiometry, IEEE Journal of Selected Topics in Applied Earth Observations and Remote Sensing, 14, 11 439–11 449, https://doi.org/10.1109/jstars.2021.3124229, 2021.

https://doi.org/10.5194/egusphere-2022-899
Preprint. Discussion started: 14 September 2022

Mousavi, M., Colliander, A., Miller, J., and Kimball, J. S.: A Novel Approach to Map the Intensity of Surface Melting on the Antarctica Ice Sheet Using SMAP L-Band Microwave Radiometry, IEEE Journal of Selected Topics in Applied Earth Observations and Remote Sensing, 15, 1724–1743, https://doi.org/10.1109/jstars.2022.3147430, 2022.

Naeimi, V., Scipal, K., Bartalis, Z., Hasenauer, S., and Wagner, W.: An Improved Soil Moisture Retrieval Algorithm for ERS and METOP Scatterometer Observations, IEEE Transactions on Geoscience and Remote Sensing, 47, 1999–2013, https://doi.org/10.1109/tgrs.2008.2011617, 2009.

Naeimi, V., Paulik, C., Bartsch, A., Wagner, W., Kidd, R., Park, S. E., Elger, K., and Boike, J.: ASCAT Surface State Flag (SSF): Extracting Information on Surface Freeze/Thaw Conditions From Backscatter Data Using an Empirical Threshold-Analysis Algorithm, IEEE Transactions on Geoscience and Remote Sensing, 50, 2566–2582, https://doi.org/10.1109/TGRS.2011.2177667, 2012.

Nagler, T. and Rott, H.: Retrieval of Wet Snow by Means of Multitemporal SAR Data, IEEE Transactions on Geoscience and Remote Sensing, 38, 754–765, 2000.

Nagler, T., Rott, H., Ripper, E., Bippus, G., and Hetzenecker, M.: Advancements for Snowmelt Monitoring by Means of Sentinel-1 SAR, Remote Sensing, 8, 348, https://doi.org/10.3390/rs8040348, 2016.

Pan, C. G., Kirchner, P. B., Kimball, J. S., Kim, Y., and Du, J.: Rain-on-snow events in Alaska, their frequency and distribution from satellite observations, Environmental Research Letters, 13, 075 004, https://doi.org/10.1088/1748-9326/aac9d3, 2018.

Pellarin, T., Mialon, A., Biron, R., Coulaud, C., Gibon, F., Kerr, Y., Lafaysse, M., Mercier, B., Morin, S., Redor, I., Schwank, M., and Völksch, I.: Three years of L-band brightness temperature measurements in a mountainous area: Topography, vegetation and snowmelt issues, Remote Sensing of Environment, 180, 85–98, https://doi.org/10.1016/j.rse.2016.02.047, 2016.

Potin, P.: Sentinel-1 User Handbook, ESA, issue 1, rev 0 edn., https://sentinel.esa.int/documents/247904/685163/Sentinel-1_User_Handbook, 2013.

Potin, P., Rosich, B., Roeder, J., and Bargellini, P.: Sentinel-1 Mission operations concept, in: 2014 IEEE Geoscience and Remote Sensing Symposium, pp. 1465–1468, https://doi.org/10.1109/IGARSS.2014.6946713, 2014.

Putkonen, J. and Roe, G.: Rain-on-Snow Events Impact Soil Temperatures and Affect Ungulate Survival, Geophysical Research Letters, 30, 1188, 2003.

Rautiainen, K., Parkkinen, T., Lemmetyinen, J., Schwank, M., Wiesmann, A., Ikonen, J., Derksen, C., Davydov, S., Davydova, A., Boike, J., Langer, M., Drusch, M., and Pulliainen, J.: SMOS prototype algorithm for detecting autumn soil freezing, Remote Sensing of Environment, 180, 346–360, https://doi.org/10.1016/j.rse.2016.01.012, 2016.

Raynolds, M. K., Walker, D. A., Balser, A., Bay, C., Campbell, M., Cherosov, M. M., Daniëls, F. J., Eidesen, P. B., Ermokhina, K. A., Frost, G. V., Jedrzejek, B., Jorgenson, M. T., Kennedy, B. E., Kholod, S. S., Lavrinenko, I. A., Lavrinenko, O. V., Magnússon, B., Matveyeva, N. V., Metúsalemsson, S., Nilsen, L., Olthof, I., Pospelov, I. N., Pospelova, E. B., Pouliot, D., Razzhivin, V., Schaepman-Strub, G., Šibík, J., Telyatnikov, M. Y., and Troeva, E.: A raster version of the Circumpolar Arctic Vegetation Map (CAVM), Remote Sensing of Environment, 232, 111 297, https://doi.org/10.1016/j.rse.2019.111297, 2019.

Schubert, A., Miranda, N., Geudtner, D., and Small, D.: Sentinel-1A/B Combined Product Geolocation Accuracy, Remote Sensing, 9, 607, https://doi.org/10.3390/rs9060607, 2017.

Schwank, M., Mätzler, C., Wiesmann, A., Wegmäller, U., Pulliainen, J., Lemmetyinen, J., Rautiainen, K., Derksen, C., Toose, P., and Drusch, M.: Snow Density and Ground Permittivity Retrieved from L-Band Radiometry: A Synthetic Analysis, IEEE Journal of Selected Topics in Applied Earth Observations and Remote Sensing, 8, 3833–3845, https://doi.org/10.1109/jstars.2015.2422998, 2015.

https://doi.org/10.5194/egusphere-2022-899
Preprint. Discussion started: 14 September 2022

Semmens, K. A., Ramage, J., Bartsch, A., and Liston, G. E.: Early snowmelt events: detection, distribution, and significance in a major sub-arctic watershed, Environmental Research Letters, 8, 014 020, https://doi.org/10.1088/1748-9326/8/1/014020, 2013.

Serreze, M. C., Gustafson, J., Barrett, A. P., Druckenmiller, M. L., Fox, S., Voveris, J., Stroeve, J., Sheffield, B., Forbes, B. C., Rasmus, S., Laptander, R., Brook, M., Brubaker, M., Temte, J., McCrystall, M. R., and Bartsch, A.: Arctic rain on snow events: bridging observations to understand environmental and livelihood impacts, Environmental Research Letters, 16, 105 009, https://doi.org/10.1088/1748-9326/ac269b, 2021.

Sokolov, A. A., Sokolova, N. A., Ims, R. A., Brucker, L., and Ehrich, D.: Emergent Rainy Winter Warm Spells May Promote Boreal Predator Expansion into the Arctic, ARCTIC, 69, https://doi.org/10.14430/arctic4559, 2016.

Spreen, G., Kaleschke, L., and Heygster, G.: Sea ice remote sensing using AMSR-E 89-GHz channels, Journal of Geophysical Research, 113, https://doi.org/10.1029/2005jc003384, 2008.

Tao, S., Ao, Z., Wigneron, J.-P., Saatchi, S., Ciais, P., Chave, J., Toan, T. L., Frison, P.-L., Hu, X., Chen, C., Fan, L., Wang, M., Zhu, J., Zhao, X., Li, X., Liu, X., Su, Y., Hu, T., Guo, Q., Wang, Z., Tang, Z., Liu, Y., and Fang, J.: C-band Scatterometer (CScat): the first global long-term satellite radar backscatter data set with a C-band signal dynamic, Earth Syst. Sci. Data Discuss., https://doi.org/10.5194/essd-2022-264, 2022.

Treharne, R., Bjerke, J. W., Tømmervik, H., and Phoenix, G. K.: Extreme event impacts on CO2 fluxes across a range of high latitude, shrub-dominated ecosystems, Environmental Research Letters, 15, 104 084, https://doi.org/10.1088/1748-9326/abb0b1, 2020.

Ulaby, F. T., Moore, R. K., and Fung, A. K.: Microwave Remote Sensing. Active and Passive, Vol. III, Artech House, Inc, 1986.

Vickers, H., Malnes, E., and Eckerstorfer, M.: A Synthetic Aperture Radar Based Method for Long Term Monitoring of Seasonal Snowmelt and Wintertime Rain-On-Snow Events in Svalbard, Frontiers in Earth Science, 10, https://doi.org/10.3389/feart.2022.868945, 2022.

Westermann, S., Boike, J., Langer, M., Schuler, T. V., and Etzelmüller, B.: Modeling the impact of wintertime rain events on the thermal regime of permafrost, The Cryosphere, 5, 945–959, https://doi.org/10.5194/tc-5-945-2011, 2011.

Wilson, R. R., Bartsch, A., Joly, K., Reynolds, J. H., Orlando, A., and Loya, W. M.: Frequency, timing, extent, and size of winter thaw-refreeze events in Alaska 2001–2008 detected by remotely sensed microwave backscatter data, Polar Biology, 36, 419–426, https://doi.org/10.1007/s00300-012-1272-6, 2012.

Woodhouse, I.: Introduction to Microwave Remote Sensing, Taylor & Francis, New York:, 2006.

https://doi.org/10.5194/egusphere-2022-899
Preprint. Discussion started: 14 September 2022

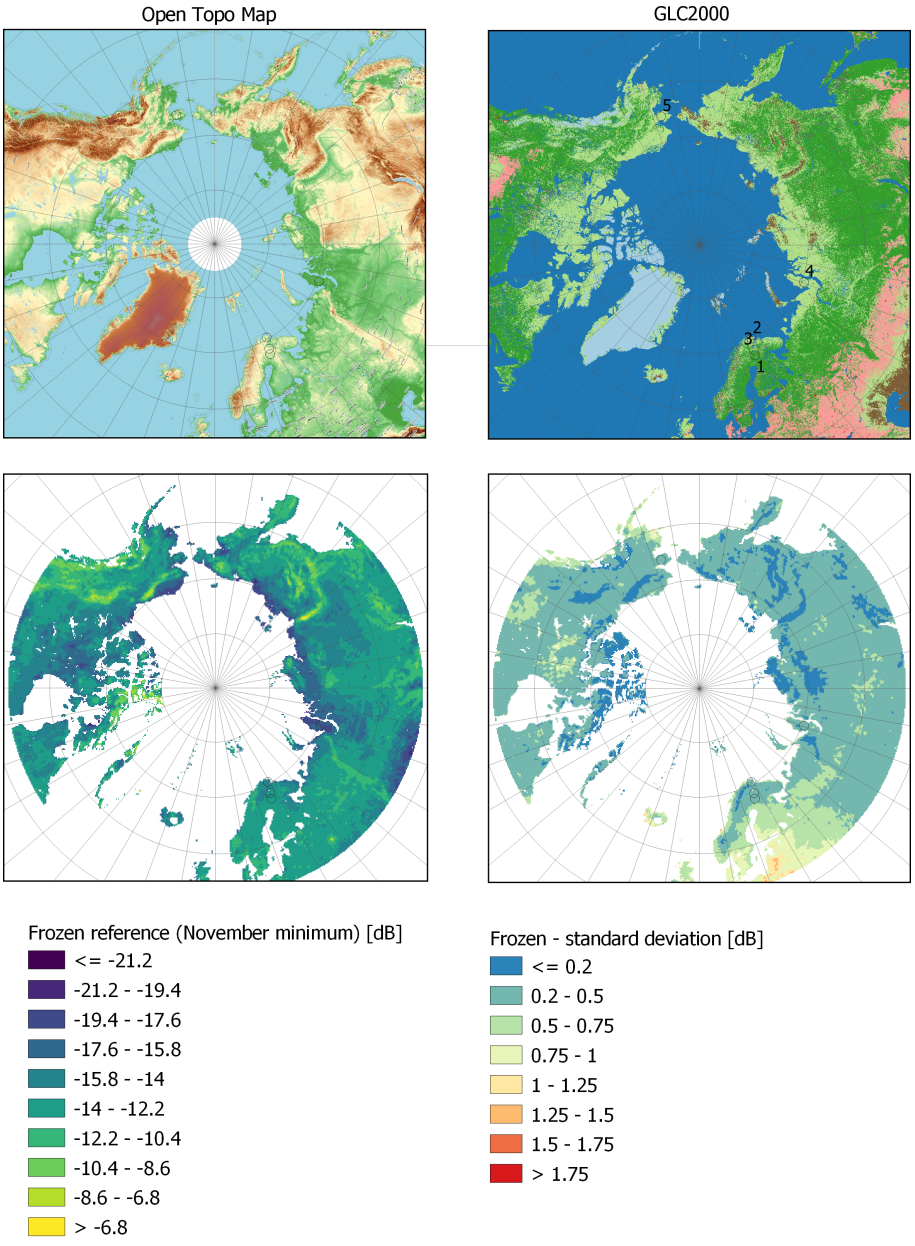

Figure 2. Metop ASCAT characteristics considered for ROS retrieval: Frozen soil reference (lower left) and standard deviation for November to February (lower right) for σ^0. Upper left: digital terrain model (source: ©OpenStreetMap-Contributors, SRTM | Mapview: ©OpenTopoMap (CC-BY-SA)), upper right: Landcover (source: Global Land Cover 2000 database. European Commission, Joint Research Centre, 2003; dark green - forest, bright green - shrubs to sparse vegetation, brown - bare, grey - burned forest, coral - cultivated, red - artificial). Circles: in situ and rain on snow case study sites: 1 - Sodankylä, 2 - Varanger peninsula/Upper Komagdalen, 3 - Saariselkä/Niilanpää, 4 - Yamal peninsula, 5 - Seward peninsula.

https://doi.org/10.5194/egusphere-2022-899
Preprint. Discussion started: 14 September 2022

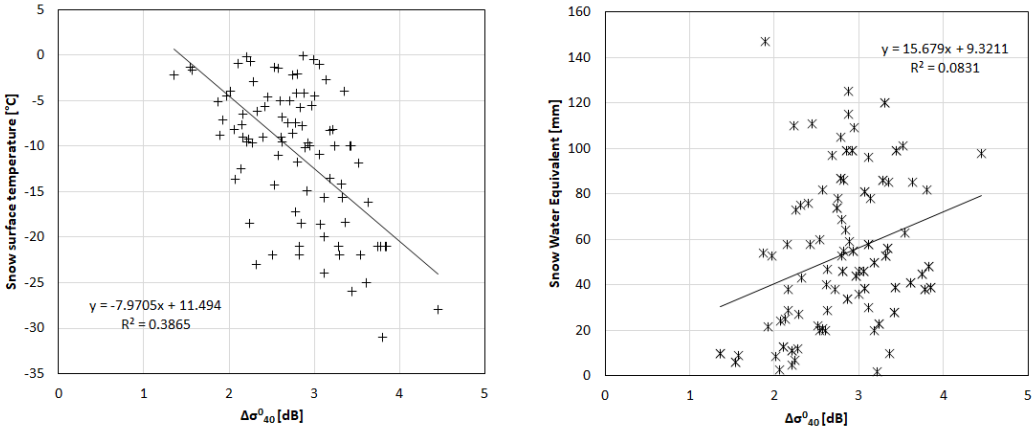

Figure 3. Comparison of Metop ASCAT C-VV $\Delta\sigma^0$ with (a) snow surface temperature and (b) snow water equivalent. Source: snow pit data at Sodankylä BOG site 2009-2015, temperatures below 0°C and SWE > 0.

https://doi.org/10.5194/egusphere-2022-899
Preprint. Discussion started: 14 September 2022

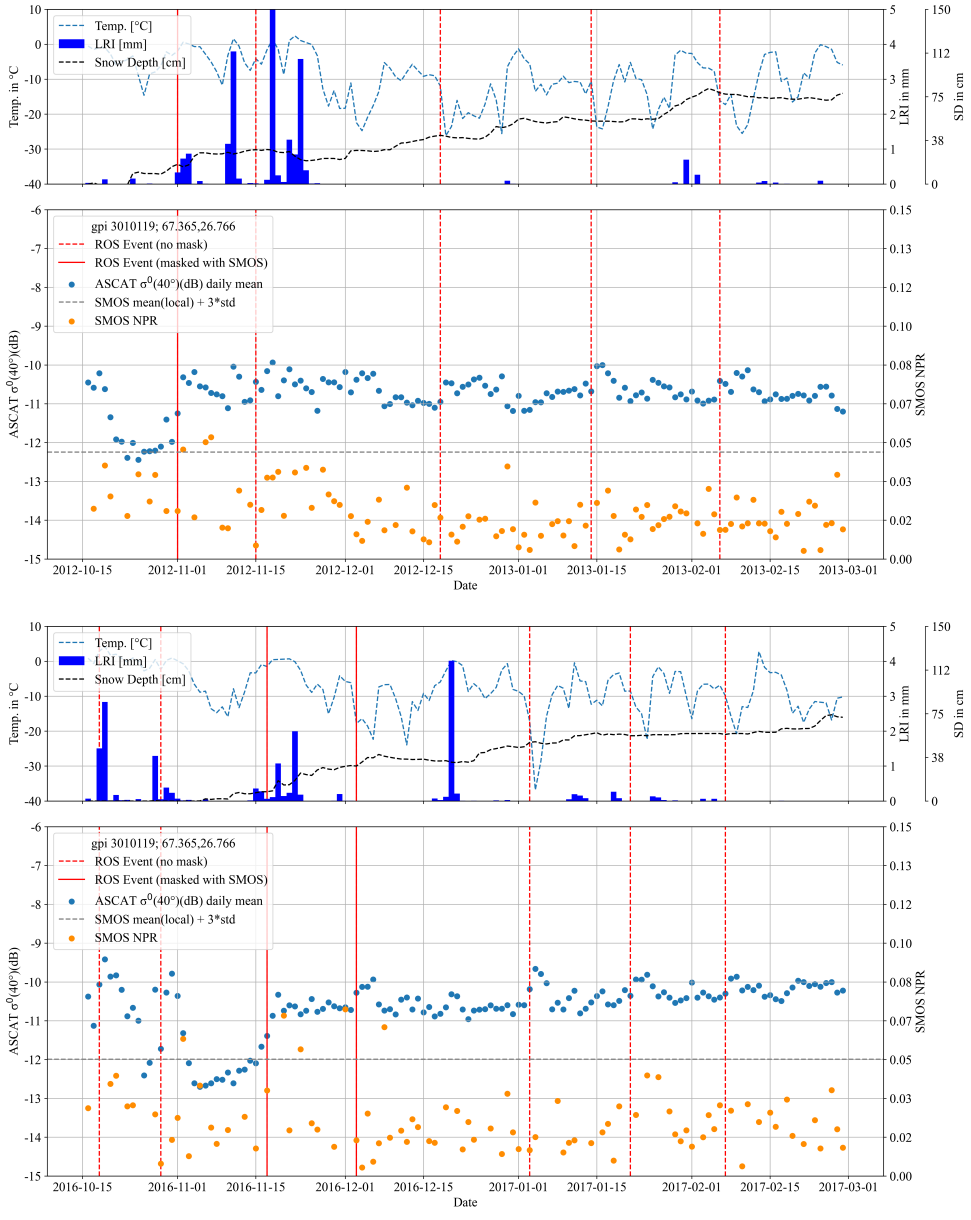

Figure 4. Examples of the influence of temperature drops on the rain-on-snow detection based on ASCAT for Sodankylä. Liquid precipitation (LRI) is shown together with air temperature and snow depth (SD) from the Automatic Weather Station for two selected winter periods. SMOS NPR and the masking threshold (derived from local mean NPR and the high latitude standard deviation, see Table 2) is shown in addition as grey horizontal dashed line. Vertical lines represent potential rain-on-snow events based on ASCAT only, with solid lines for periods confirmed with high SMOS NPR (wet snow).

https://doi.org/10.5194/egusphere-2022-899
Preprint. Discussion started: 14 September 2022

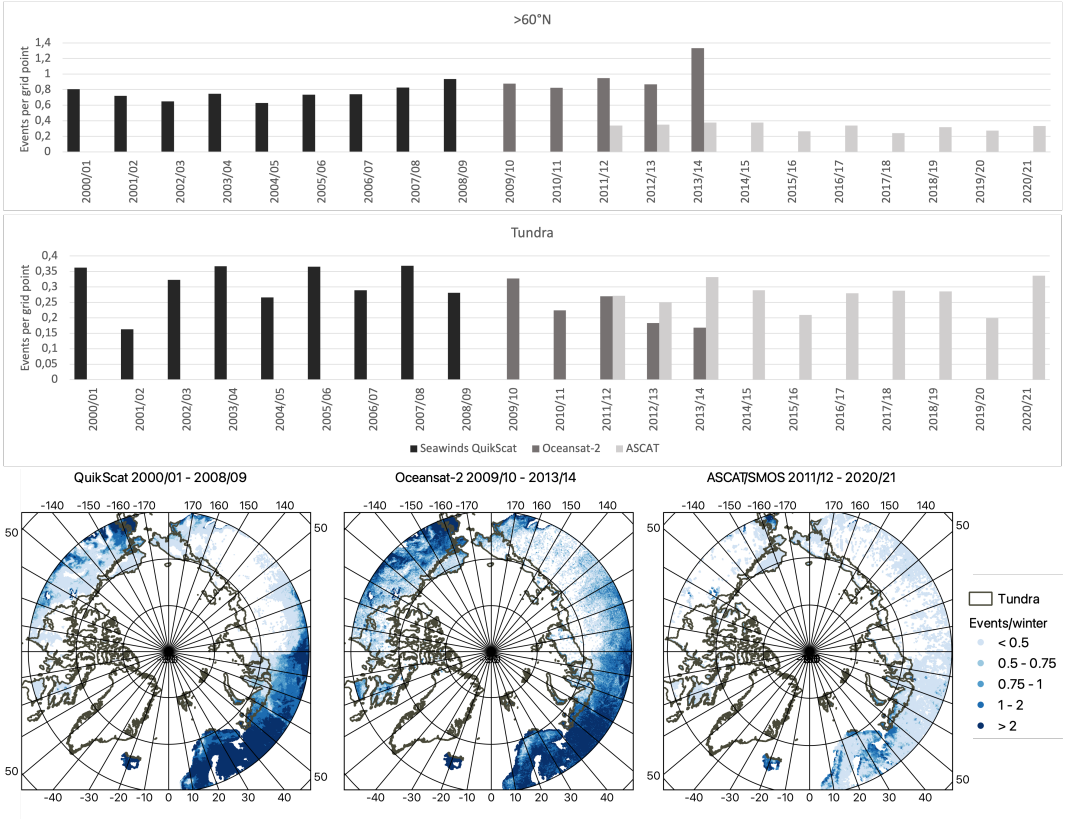

Figure 5. Top and centre: Number of events per winter and grid cell (resampled to QuikScat 10 x 10 km grid) for overlap area of full extend (excludes Greenland and masked areas in the ASCAT/SMOS results) as well as for tundra only. Bottom: Winter averages and tundra extend (source CAVM, Raynolds et al. (2019)).

https://doi.org/10.5194/egusphere-2022-899
Preprint. Discussion started: 14 September 2022

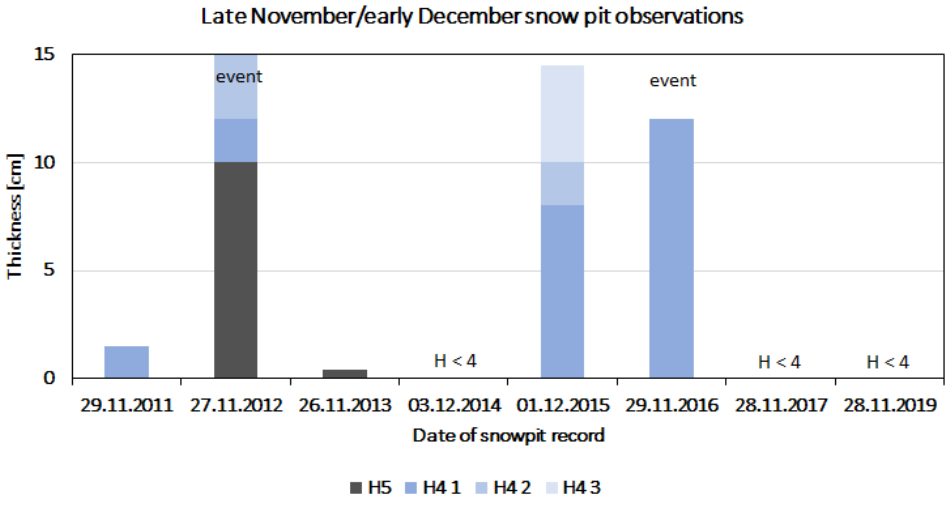

Figure 6. Snow pit observations at the IOA site (Sodankylä) in late November/early December. 'event' indicates years with rain-on-snow event (see Figure 4). Layer thickness is cumulative and shown for all layers with hardness ≥ 4.

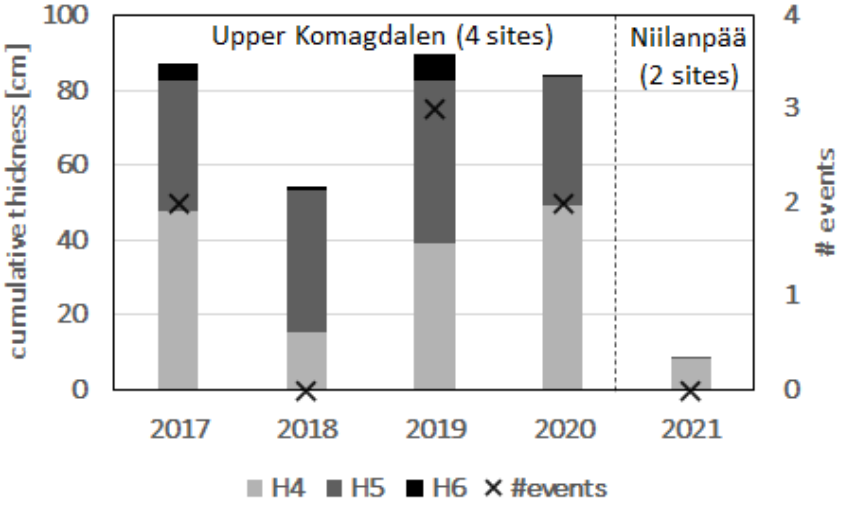

Figure 7. Average cumulative ice layer (for definition see table 1) thickness in snowpits at central Komagdalen, Varanger (18.03.2017, 13.03.2018, 20.03.2019, 18.03.2020) and at Saariselkä (18.03.2021). Separation for hardness (H) classes and number of potential rain-on-snow events between November and February. Snow depth range: 70-162cm at Komagdalen and 42-66cm at Niilanpää.

https://doi.org/10.5194/egusphere-2022-899
Preprint. Discussion started: 14 September 2022

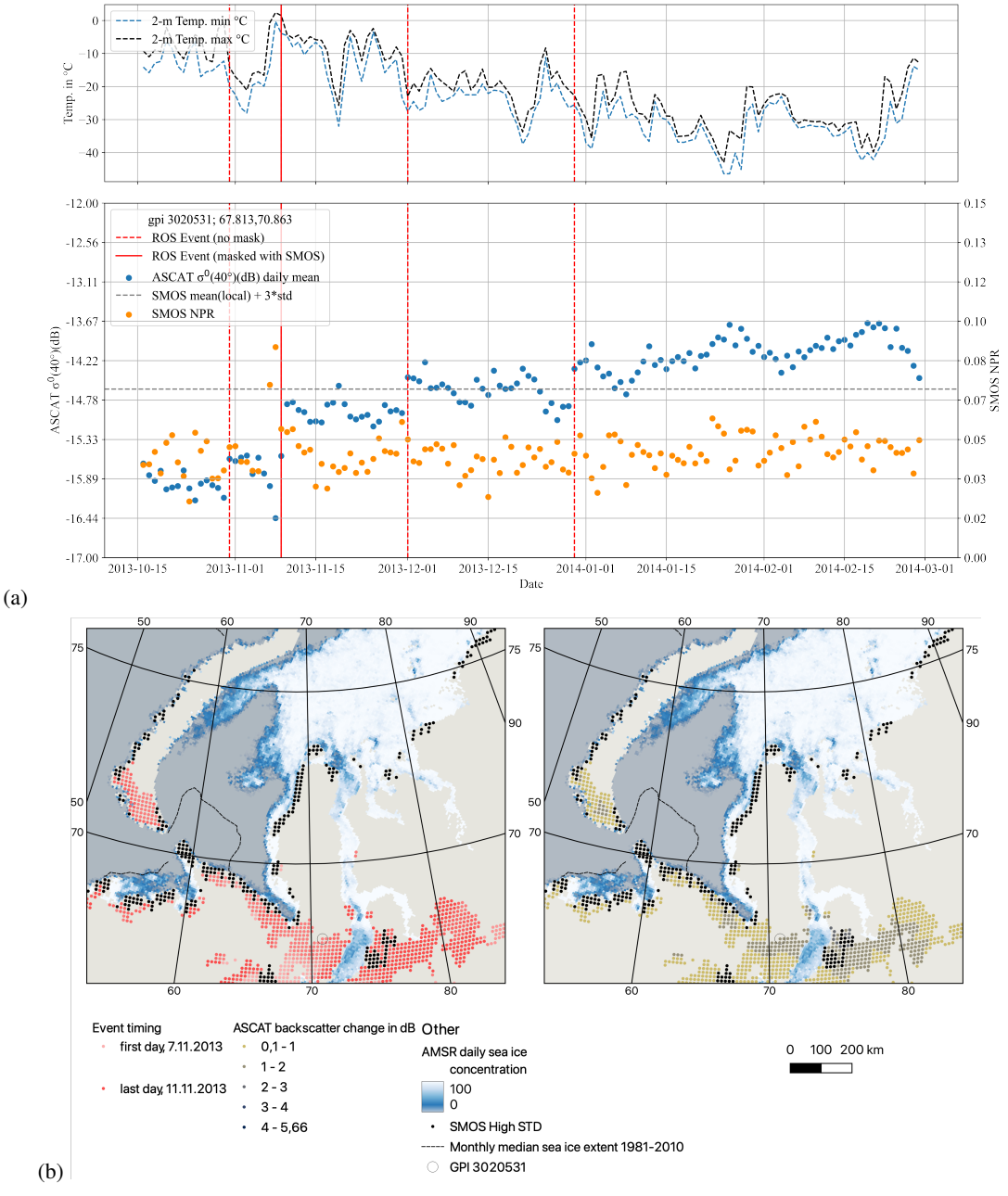

Figure 8. Example for a grid point on southern Yamal documenting the 2013 event (as described in Forbes et al. (2016)). (a) Time series of ASCAT backscatter and SMOS NPR. Air temperature data have been obtained from reanalyses data (ERA5). Only the detected event around 10th of November has been caused by a ROS (with a high SMOS NPR at the same time). All other events correspond to temperature drops. For location see black circle in (b). b) Grid points with an event in November 2013 and sea ice concentration (9.11.2013 and long-term November average, source: University of Bremen, Spreen et al. (2008)). Left: event date by grid point, right: ASCAT $\Delta\sigma^0$.

https://doi.org/10.5194/egusphere-2022-899
Preprint. Discussion started: 14 September 2022

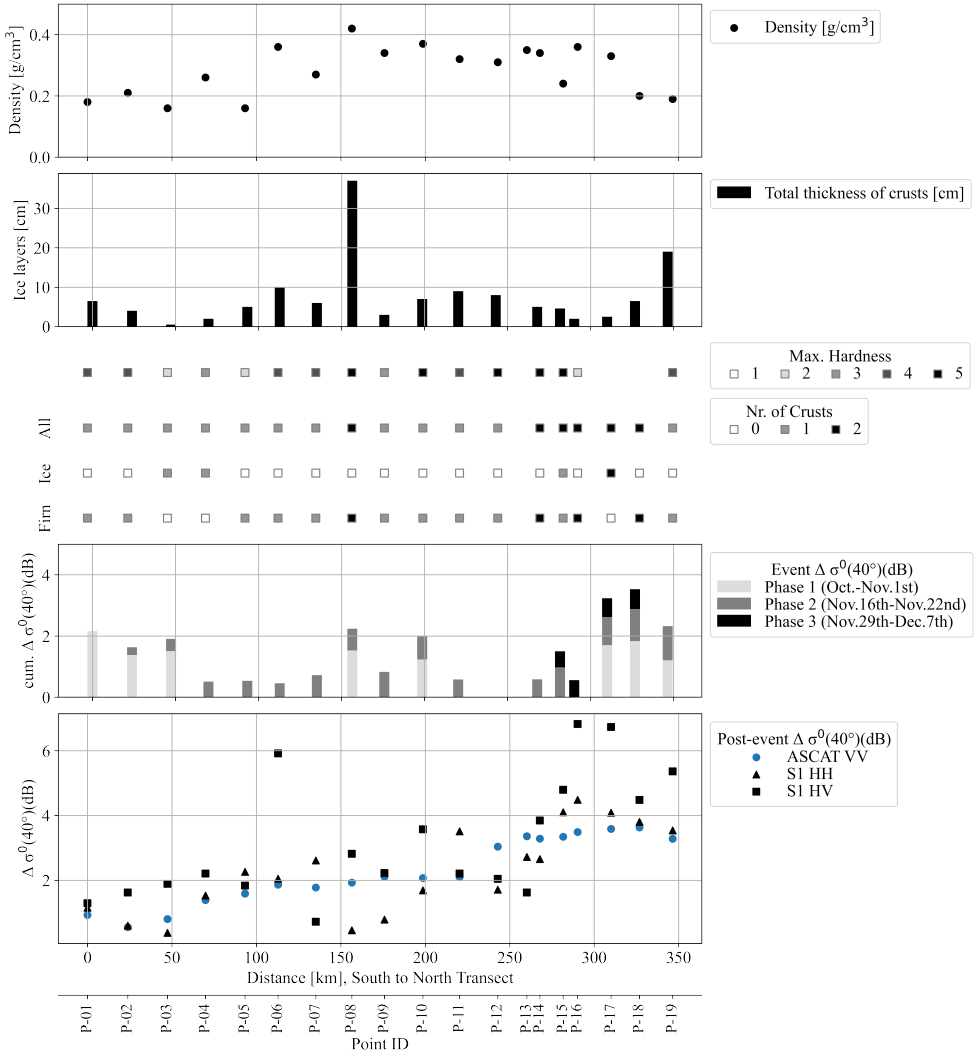

Figure 9. Documentation of snow conditions after the ROS events across Yamal end of 2020. Measurements obtained in February 2021 (five snow pits per site; average snow density, maximum crust type and hardness and thickness of crust). ASCAT $\Delta\sigma^0$ along the in situ transect by event and σ^0 from ASCAT and Sentinel-1 during the week after the last event. For location of points see Figure 10. No events available for near coast points 12 and 13 due to SMOS data gap.

https://doi.org/10.5194/egusphere-2022-899
Preprint. Discussion started: 14 September 2022

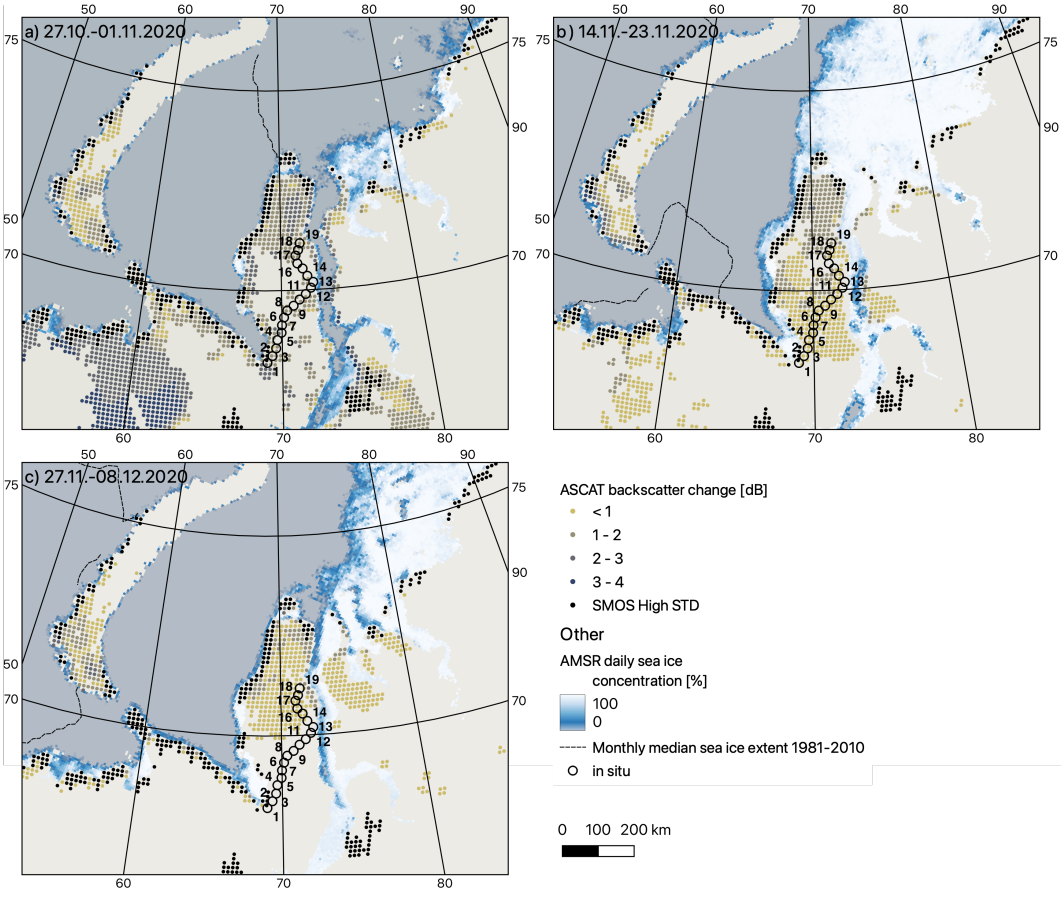

Figure 10. Cumulative ASCAT $\Delta\sigma^0$ (in dB, incl. SMOS masking for wet snow and RFI) and AMSR sea ice extent (source: University of Bremen, Spreen et al. (2008)) for event series in early winter 2020 on the Yamal peninsula. a) 27.10.-01.11.2020, sea ice extent 26.10.2020 and October monthly mean, b) 14.11.-23.11.2020, sea ice extent 13.11.2020 and November monthly mean, c) 27.11.-8.12.2020., sea ice extent 27.11.2020 and December monthly mean. Location of in situ points for snow surveys in February 2021 (Figure 9).

https://doi.org/10.5194/egusphere-2022-899
Preprint. Discussion started: 14 September 2022

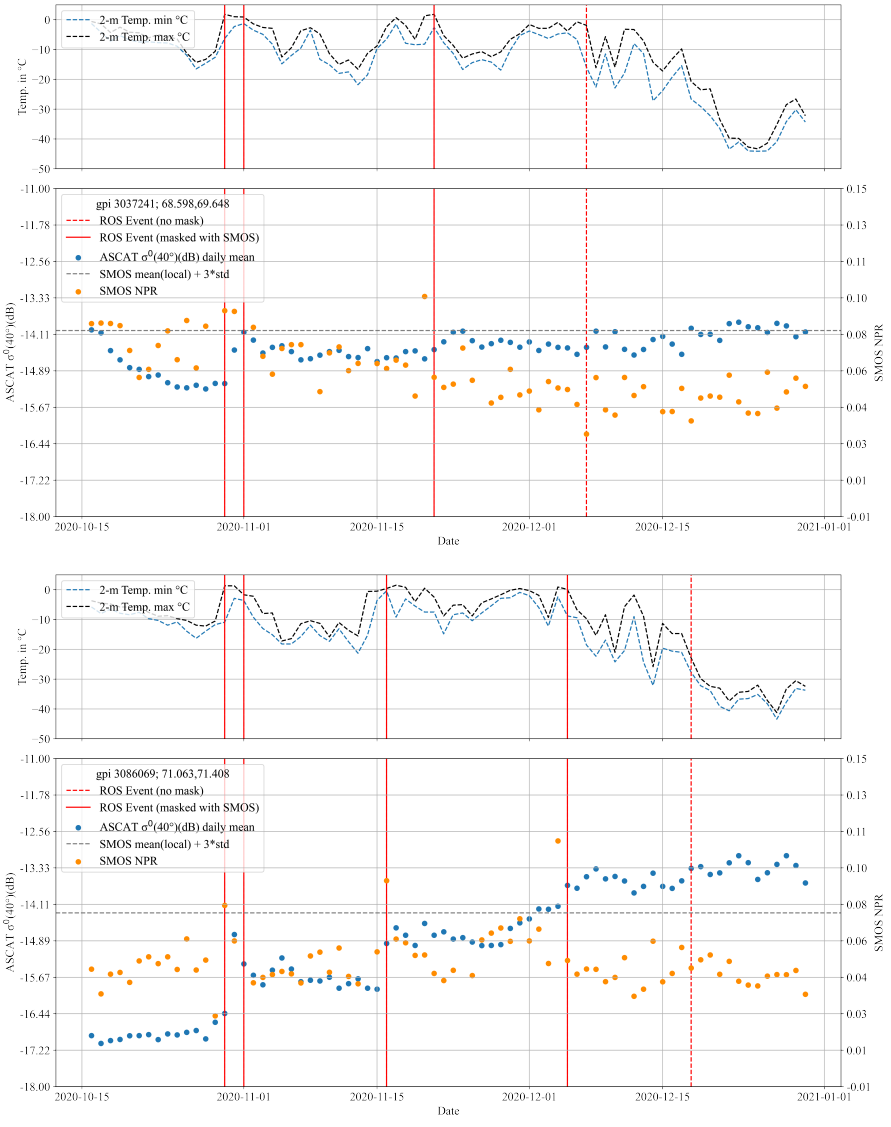

Figure 11. Time series examples for the event series in early winter 2020 on the Yamal peninsula, a) south, #3 , b) north #18. For location see Figure 10.

https://doi.org/10.5194/egusphere-2022-899
Preprint. Discussion started: 14 September 2022

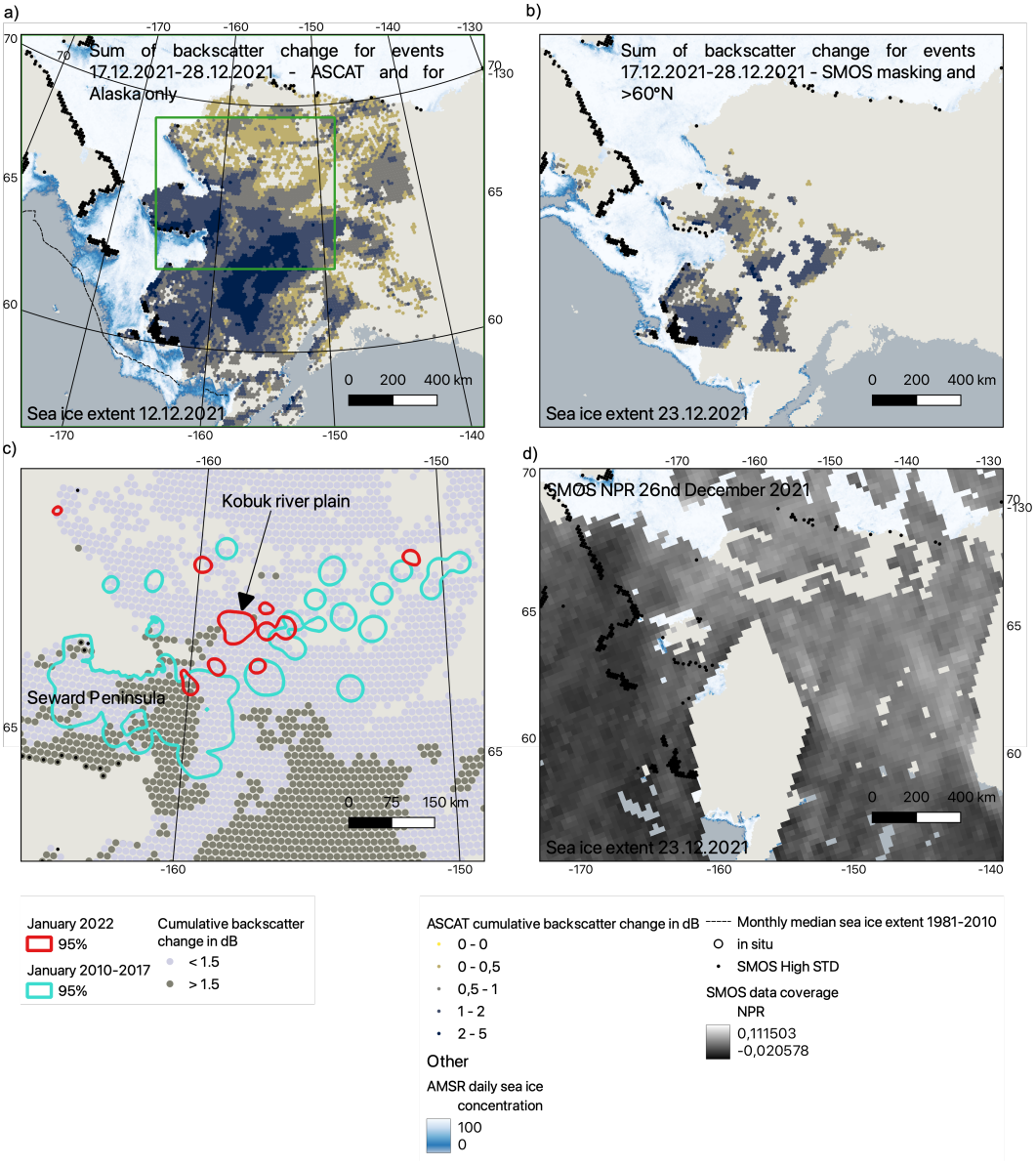

Figure 12. Rain on snow event in Alaska December 2021: a) cumulative ASCAT $\Delta\sigma^0$ for both events before masking with SMOS and sea ice extent before the first event; green rectangle - extent of map (c); b) after masking and sea ice extent at the beginning of the second event, c) separation of cumulative ASCAT $\Delta\sigma^0$ > 1dB and areas of caribou presence January 2010-2017 versus 2022; d) example for SMOS NPR availability from a single day. Source of sea ice data: University of Bremen, Spreen et al. (2008).

https://doi.org/10.5194/egusphere-2022-899
Preprint. Discussion started: 14 September 2022

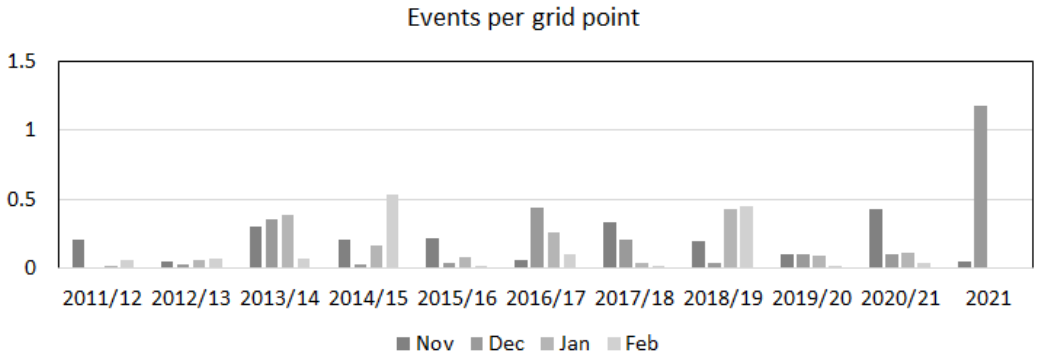

Figure 13. Number of events per grid point for the Seward Peninsula (for location see Figure 12). SMOS masking (wet snow and RFI) has been applied.